AD-A174 691 HOMOGENIZING SURFACE AND SATELLITE OBSERVATIONS OF CLOUD(U) EUROPEAN OFFICE OF AEROSPACE RESEARCH AND DEVELOPMENT FPO NEW A HENDERSON-SELLERS ET AL 1/1

UNCLASSIFIED 28 NOV 86 EOARD-TR-87-01 AFOSR-85-0299 F/G 4/1 NL

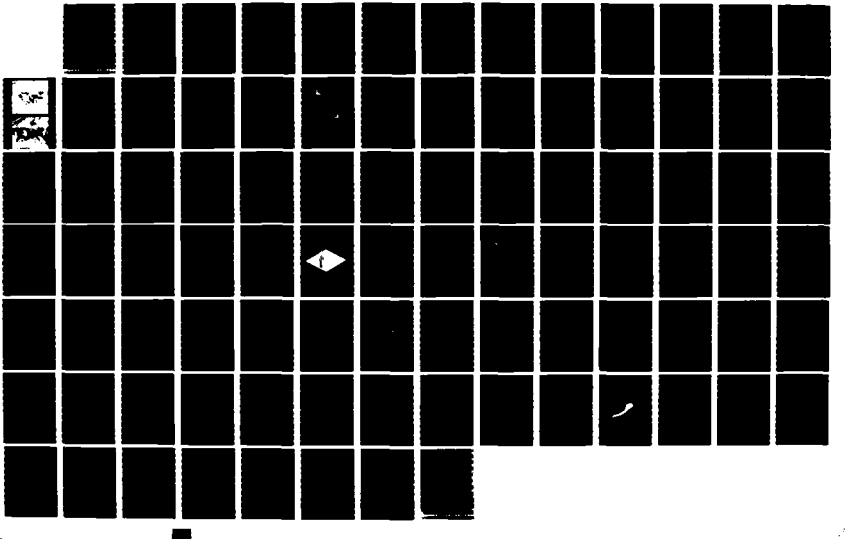

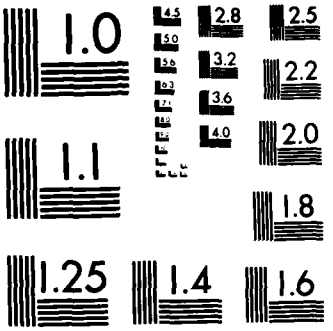

(2)

Contract / Grant Number AFOSR-85-0299

HOMOGENIZING SURFACE AND SATELLITE OBSERVATIONS OF CLOUD

A. Henderson-Sellers and A. Goodman
Department of Geography,
University of Liverpool,
Liverpool, U.K.

28 November 1986

Interim Scientific Report , 1 October 1985 -
30 September 1986

Approved for public release; distribution unlimited

Prepared for

EUROPEAN OFFICE OF AEROSPACE RESEARCH AND DEVELOPMENT
London, England.

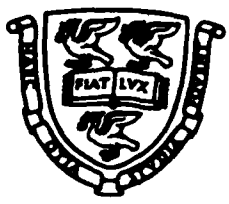

86 12 01 015

DISCLAIMER NOTICE

THIS DOCUMENT IS BEST QUALITY PRACTICABLE. THE COPY FURNISHED TO DTIC CONTAINED A SIGNIFICANT NUMBER OF PAGES WHICH DO NOT REPRODUCE LEGIBLY.

EOARD-TR-87-21

This report has been reviewed by the EOARD Information Office and is releasable to the National Technical Information Service (NTIS). At NTIS it will be releasable to the general public, including foreign nations.

This technical report has been reviewed and is approved for publication.

Owen R. Coté

OWEN R. COTE'
Chief, Geophysics and Space

Robert C Winn

ROBERT C. WINN, Lt Colonel, USAF
Chief Scientist

REPORT DOCUMENTATION PAGE		READ INSTRUCTIONS BEFORE COMPLETING FORM
1. Report Number	2. Govt Accession No. ADA174691	3. Recipient's Catalog Number
4. Title (and Subtitle) Homogenizing surface and satellite observations of cloud.		5. Type of Report & Period Covered Interim, 1 October 85 - 30 September 86. 6. Performing Org. Report Number
7. Author(s) Ann Henderson-Sellers and Alan Goodman		8. Contract or Grant Number AFSOR-85-0299
9. Performing Organization Name and Address Department of Geography, University of Liverpool, P.O. Box 147, Liverpool, L69. 3BX.		10. Program Element, Project, Task Area & Work Unit Numbers Program element: 61102F Project/Task: 2301/D1
11. Controlling Office Name and Address EOARD 223/231 Old Marylebone Road, London, NW1, 5TH U.K.		12. Report Date 28 November 1986 13. Number of Pages 82
14. Monitoring Agency Name and Address		15.
16. & 17. Distribution Statement Approved for public release; distribution unlimited.		
18. Supplementary Notes		
19. Key Words Cloud retrieval, satellite radiances, surface observations of clouds.		

20. Abstract

The major types of cloud retrieval algorithms are reviewed with special emphasis being placed upon recent ~~(i.e. post 1981/82)~~ developments and novel techniques. Satellite-based retrieval algorithms can be grouped into three classes: threshold methods, statistical procedures and radiative transfer techniques although each algorithm depends upon implicit, if not overt, inversion of the radiative transfer equation. The fourth type of retrieval differs very considerably from the satellite-based techniques as it depends upon surface-based measurements which are generally, but not always, human rather than computer based. There is a tendency to assume that surface-based observations, especially of total cloud, are "correct" but that they may differ from satellite-based retrievals because of the differences in viewing

20. Abstract cont,d.....

geometry. Actually the literature reveals surprisingly few intercomparison studies. None of the satellite-based techniques have yet been well validated in a variety of situations while surface-based observations are made in all terrain and climate regimes. Overall there seems to be good reason to believe that surface-based observations of cloud amount and especially of low cloud amount, character and base height can add significantly to satellite-based retrieval algorithms. (GREAT BRITAIN)

Contents

1 Introduction

This report comprises the first stage of a Ph.D. study. The aim is to review the basis of cloud observation techniques laying particular emphasis on satellite-based retrievals. Since the early 1980s there have been a number of developments in remote sensing of cloud characteristics and these are reviewed here. It is clear that whilst many of the more novel techniques offer additional insight into cloud features none of them have yet been adequately validated.

The U.S. Air Force's nephanalyses, 3D Neph and RT Neph have been excluded intentionally from this review for two reasons: (i) they are based on a range of data from a variety of sources and (ii) an adequate description of the newer, current algorithm (RT Neph) is still awaited. Despite this exclusion our conclusions (see Sections 3 and 4) suggest that RT Neph may well be benefitting greatly from the inclusion of conventional as well as satellite-based observations.

With the advent of satellite technology, we have been provided with the facility to observe clouds from above as well as below. Due mainly to their vastly superior areal coverage the last two decades have witnessed a sustained effort in utilising remotely sensed radiation from various regions of the electromagnetic spectrum to derive cloud parameters relevant to meteorological and climatological studies. The human eye, though still employed in a daily observational sense has been forced to take a secondary role compared to that of the satellites. The development and use of sophisticated climate models has taken into consideration the radiative effects of the global cloud field and, along with increasing awareness of the significant role the various cloud types play in determining the

Earth's radiation budget, has contributed to the need for global cloud coverage information which can, of course, only be achieved from spaceborne sensors, there being insufficient resources available to deploy the required density of surface observers, especially over the oceans.

The International Satellite Cloud Climatology Project (ISCCP) (World Climate Programme (WCP), 1982; Schiffer and Rossow, 1983, 1985) aims to provide users with a uniform global radiance climatology from which specific cloud parameters will be extracted. The method of extraction (i.e. choice of particular cloud retrieval algorithm) is of crucial importance. As will become evident, there is at present no single retrieval algorithm capable of performing all the tasks required of it and, equally important, a lack of 'truth' data sets against which results can be compared (Rossow et al., 1985). For ISCCP to be of sustained beneficial use the cloud retrieval (as well as being as accurate as possible), will need to be very precise (Table 1). In this case the accuracy of retrieval refers to the minimising of systematic errors in the reception and calibration of the satellite data. The high precision requirement defines the confidence limits of the estimated cloud parameters. Many recent algorithm developments have taken place, in many cases building on previous work to increase the sensitivity towards detection of specific cloud systems. In the following sections present-day knowledge of satellite cloud retrieval is reviewed, the main problems analysed and the feasibility of merging surface observations into the retrieved cloud fields examined in the light of recent work (e.g. Sèze et al., 1986).

When the first satellite-derived images were made available to

Table 1 Data specification for the International Satellite Cloud Climatology Project (after Rossow et al., 1985)

Parameters - Spatial and temporal averages and variances (or another statistical measure of the shape of the temporal distribution) are required for each of the following parameters.

	Precision (30-day averages)
Amounts	
Total cloud amount (fraction)*	±0.03
Cirrus cloud amount (fraction)*	±0.05
Middle cloud amount (fraction)	±0.05
Low cloud amount (fraction)*	±0.05
Deep convective cloud amount (fraction)	±0.05
Height	
Cirrus cloud-top height (km)*	±1.00
Middle level cloud-top height (km)	±1.00
Low-level cloud-top height (km)	±0.50
Deep convective cloud-top height (km)	±1.00
Cloud-Top Temperature (K) for each cloud category*	±1.00
Cloud Optical Depth	
Cloud Size Distribution	
Average Narrow Band Radiances (VIS and IR)*	

Spatial Averaging - The information is to be averaged over approximately 250 km by 250 km boxes

Time Sampling - Every 3 hours i.e. 8 times a day, centred around the synoptic observation times

Time Averaging - The global cloud climatology will consist of 30-day averages for each of the 8 observing times per day

Length of Time Series - 5 years

* highest priority

users, meteorologists were faced with a choice of either carrying out a manual analysis of the photographic image (Clapp, 1964) or devising an automated technique to process the digitized data, in order to ascertain, for example, cloud amount (Arking, 1964). Manual nephanalyses were found to consume many man-hours of time whilst at the same time incorporating an inevitable degree of subjectivity. Automated processing, although unsuccessful initially (Goodshall, 1970) is now, with the aid of modern computers, a much more efficient means of analysis, especially for quantitative determination. ISCCP will eventually provide over 1800 days worth of global data: a data archive clearly beyond the ability of manual analysts.

2 Cloud Retrieval Algorithms

All cloud retrieval algorithms comprise two basic steps, namely initial detection of cloud followed by quantitative analysis of that cloud. The first step involves separating observed radiances into either a clear or cloudy category. The methodology employed in the separation defines a particular type of algorithm. The analysis step concerns the determination of cloud properties from the observed radiances and may vary from the fitting of complex radiative transfer models in order to obtain parameterised cloud properties to the straightforward task of counting cloudy pixels to determine cloud cover fraction. Implicit in any algorithm is a set of assumptions (in effect a radiative model) characterising the relationship between the Earth's surface, the atmosphere and clouds with the satellite measurements. Algorithms may be distinguished by the type and complexity of the inherent radiative model but all are designed to retrieve cloud properties, the retrieval being dependent upon the methodology used. The accepted means of distinction is, however, the application of

detection and analysis to either groups of image pixels or individual image pixels. This latter type of algorithm is termed a threshold method whilst the former type is known as a statistical method. In addition a third type of algorithm, the radiative transfer technique can be arbitrarily defined by virtue of its differing approach to retrieval. Each category and its applications are reviewed in turn and, where possible, illustrated with reference to NOAA-7 polar orbiting data for Western Europe on 10th August 1983. The data comprise three arrays of 512 x 512 image pixels covering the latitude belt 42° to 57° North. The major weather systems present are a depression in the Bay of Biscay with associated convective disturbances on its eastern flank and an anticyclone with clearer skies over Southern Scandinavia. The images (Figure 1(a) is channel 1 [0.58 -0.68 μm] and Figure 1(b) is channel 5 [11.5 - 12.5 μm]), which are for 1425 GMT on the 10th August 1983, and the surface synoptic chart for midday on the 10th August (Figure 1(c)) indicate a range of features: fog in the North Sea, multi-level cloud over France and some clear land and ocean areas.

2.1 Threshold Techniques for Cloud Retrieval

The threshold method treats each image pixel separately, assigning to each pixel or field of view a completely clear or cloudy label according to the magnitude of the observed radiance relative to the predetermined threshold level i.e. the pixel cloud fraction, (referred to hereafter as f) equals either 0 or 1. This definition (Arking and Childs, 1985) appears to contradict that given in the ISCCP preliminary implementation plan (WCP, 1982) which states that the cloud fraction is linearly related to the difference between the

Figure 1(a) Visible (channel 1, 0.58 - 0.68 μm) image from NOAA-7 Advanced Very High Resolution Radiometer (AVHRR) taken at 1425 GMT, 10th August 1983. (Image Courtesy of University of Dundee).

Figure 1(b) As for (a) except thermal infrared (channel 4, 10.5 - 11.5 μm). (Image Courtesy of University of Dundee).

Figure 1(c) Surface synoptic chart for 1200 GMT on 10th August 1983

C.

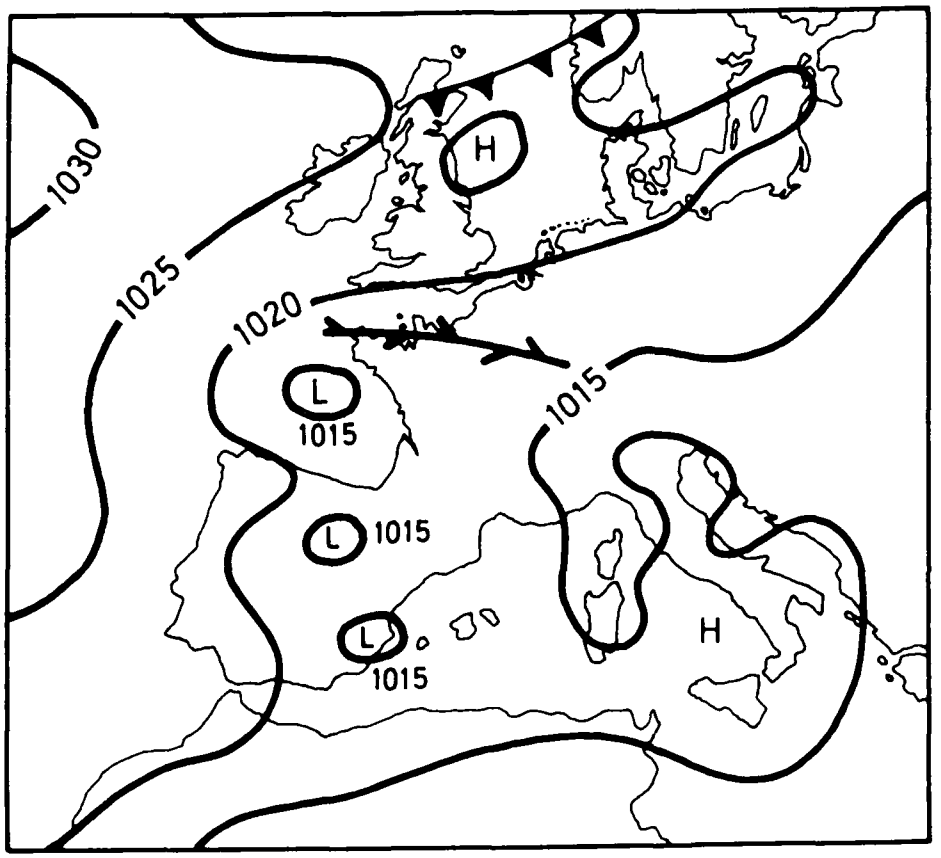

b.

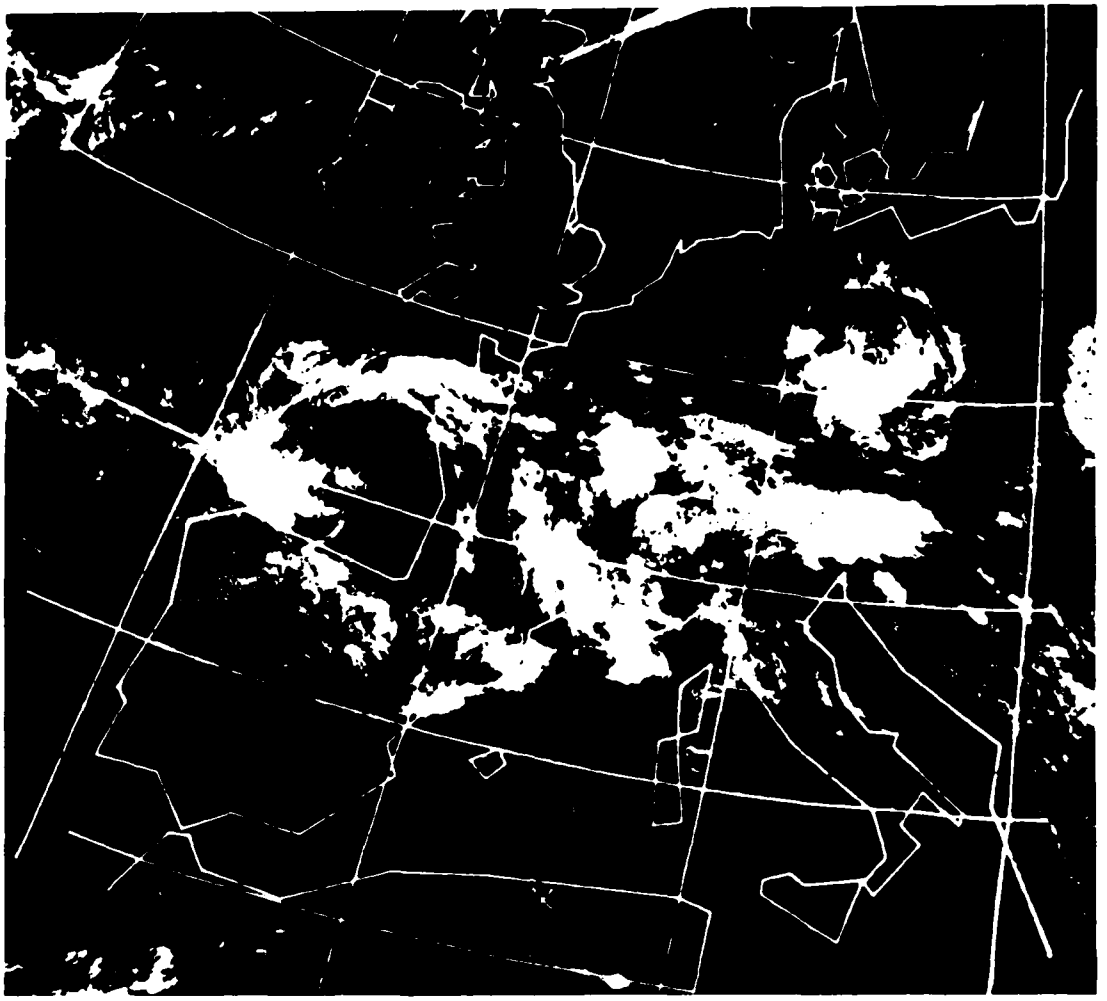

a.

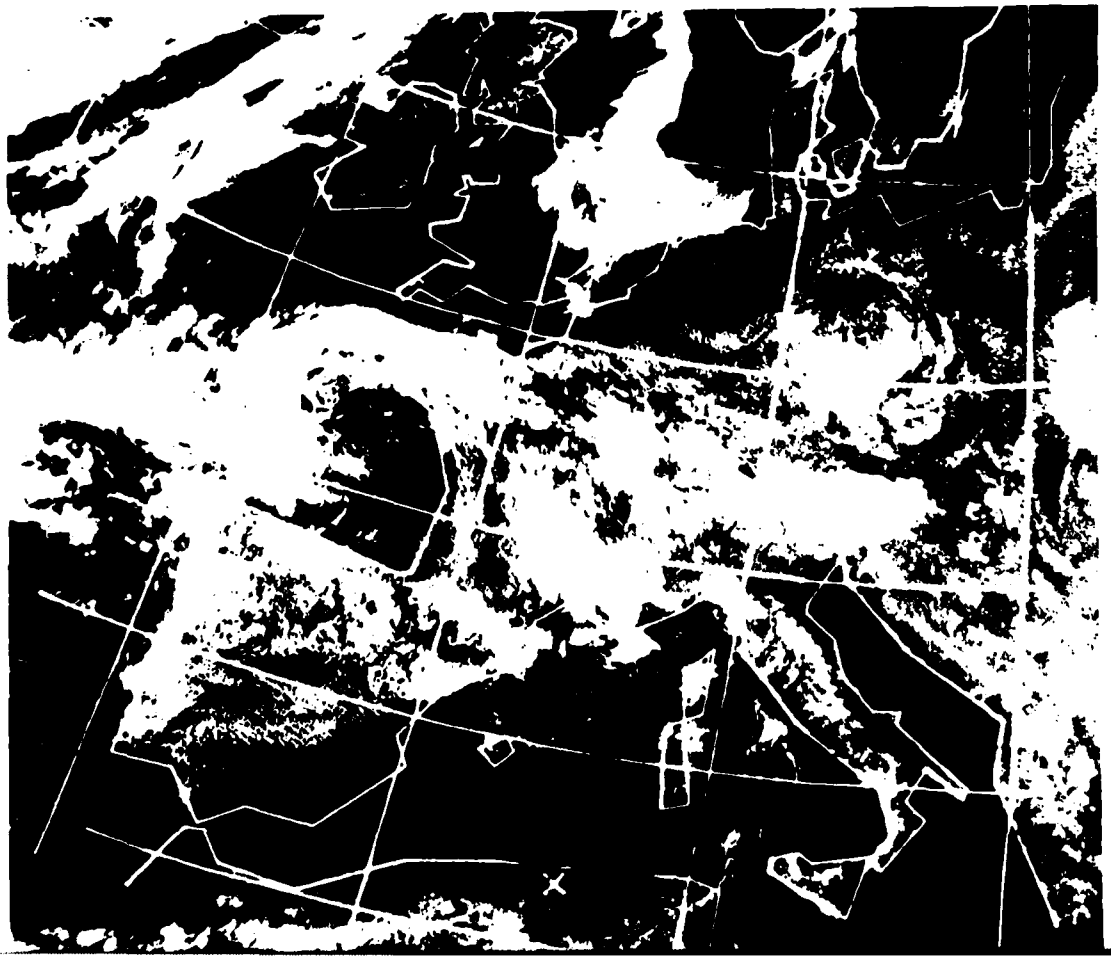

observed and threshold radiance, implying values of f intermediate between 0 and 1. However, Godshall (1970), reporting on the previous work of Barnes and Chang (1968) implied a definition consistent with the former (i.e. f = 0 or 1) and applications reported since 1982 (Liljas 1984, Wielicki and Welch, 1986) confirm this view.

A single channel threshold was originally used (e.g. Saunders and Hunt, 1980) which involved no auxiliary data to determine cloud cover, this method is termed the 'gross cloud check' in Saunders (1986). However, bispectral or double-channel thresholds are now also documented (Minnis and Harrison, 1984a,b,c and see also Ackerman and Cox, 1981). The ISCCP pilot study of 1981 (World Climate Programme 1982), aiming to establish the relative effectiveness of the then available algorithms included both single channel and bispectral thresholds in its evaluation. The single channel version defines the threshold as some increment in either visible reflectance (ΔR) or infrared brightness temperature (ΔT) from a clear sky value (R_s,T_s) so that for visible (infrared) radiances, a pixel is labelled cloudy if $R > R_s + \Delta R$ (or $T < T_s - \Delta T$). The cloud cover fraction can then be obtained by counting up all the 'cloudy' pixels whilst other parameters e.g. visible albedo, cloud top temperature can be derived from cloud radiative models and the cloudy radiance values. The clear sky and cloudy radiances form a monotonic distribution, the clear sky radiance corresponding to minimum reflectance (visible channel) or maximum brightness temperature (infrared channel). Time records of the extreme values for each pixel are examined and 15 or 30 day composite images can be constructed (e.g. see Sèze and Lesbois, 1986) where a pixel's minimum reflectance, say, is assumed to represent the clear sky reflectance for that period. In certain situations minimum

visible reflectance does not coincide temporally with maximum brightness temperature (Sèze and Desbois, 1986). The time period should be sufficiently long so as to account for any variation of surface properties and in the case of geostationary satellites it can compensate for the effects of viewing geometry (which do not alter in time). Spatial filtering of the composite image can remove any noise due to cloud contamination and then the threshold increments, typically 3% reflectance and 6 K brightness temperature can be applied.

Alternative methods of setting the threshold exist: visual inspection of the one-dimensional frequency histogram of either visible reflectances (Wielicki and Welch, 1986; Saunders, 1986) or spatial variations in the radiance field. In the former case, applied by Wielicki and Welch (1986) to fair weather cumulus fields, the reflectance histogram (Figure 2) displayed a highly uniform distribution of cloud reflectance and the cloud fraction was strongly related to the selected threshold as shown in Figure 3. In this case it was concluded that many small clouds (~100m in size) had been observed (because of the fact that reflectance is observed to increase notably with cloud size) and that reflectance across individual clouds was highly irregular. Alternatively, Saunders (1986) applied a 'dynamically controlled' threshold using several inter-related parameters to separate any cloud free peaks present from remaining cloudy radiances (Figure 4). Examination of the histograms in Figure 5 shows that in the visible case (Figure 5(a)) values of the threshold parameters m, n and T could be tuned to give an accurate cloud fraction estimate whilst in the infrared example (Figure 5(b)) the

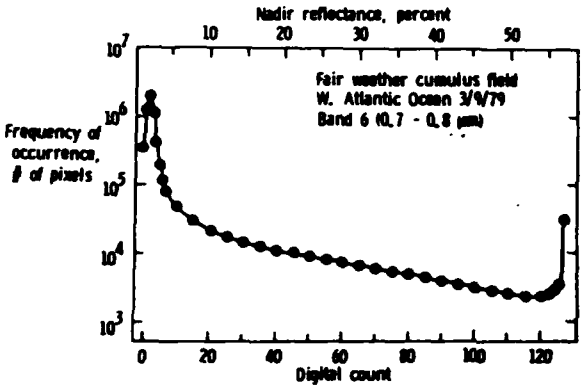

Figure 2 Histogram of Landsat digital count (i.e., reflectance) for a western Atlantic cumulus cloud field. The curve is plotted for all 127 digital count values but for simplicity selected values are shown. The equivalent nadir lambertian reflectance scale is given at the top of the figure (after Wielicki and Welch, 1986).

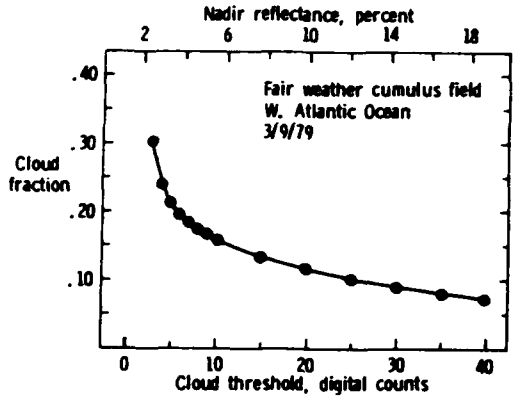

Figure 3 Cloud fraction as a function of cloud reflectance threshold for the western Atlantic cloud field (after Wielicki and Welch, 1986).

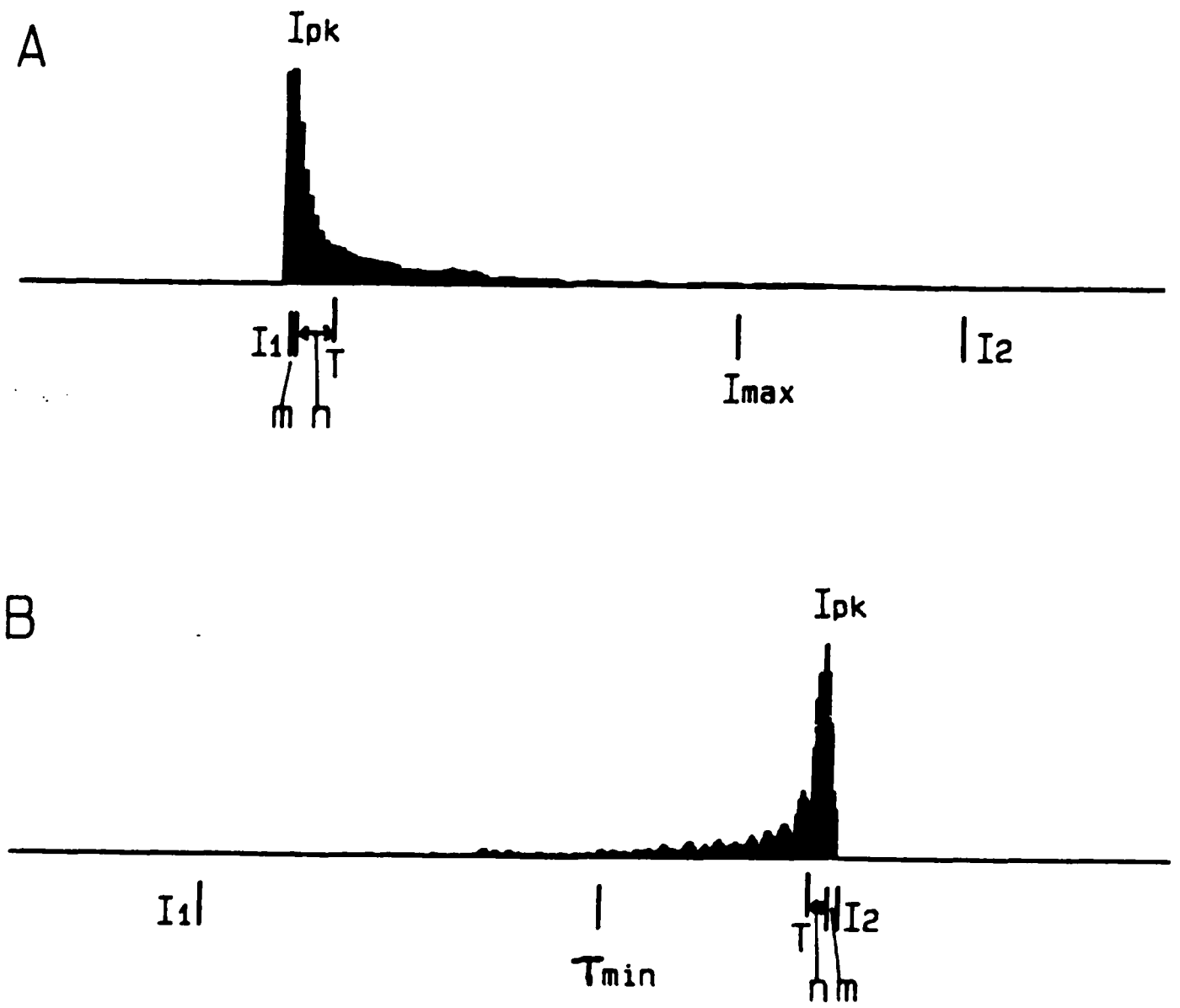

Figure 4

Examples of (A) visible (0.58 - 0.68 μm) radiance and (B) 11 micrometer brightness temperature histograms with cloud free peaks (after Saunders, 1986). The computed dynamic threshold is given as T which is determined as follows from visible (infrared) histograms: first calculate the number of radiances that constitute the peak and the value of I_{pk}. If the peak is considered to be significant then (i) determine the lower and upper limits of the histogram (I_1 and I_2 respectively). (ii) If I_1 (I_2) lies within 'm' counts of the peak and $I_{pk} < I_{max} (> T_{min})$, then the peak is assumed to be cloud free with the threshold T set at 'n' counts above I_{pk}. Values of the parameters, m, n, I_{max} and T_{min} are given in Saunders (1986).

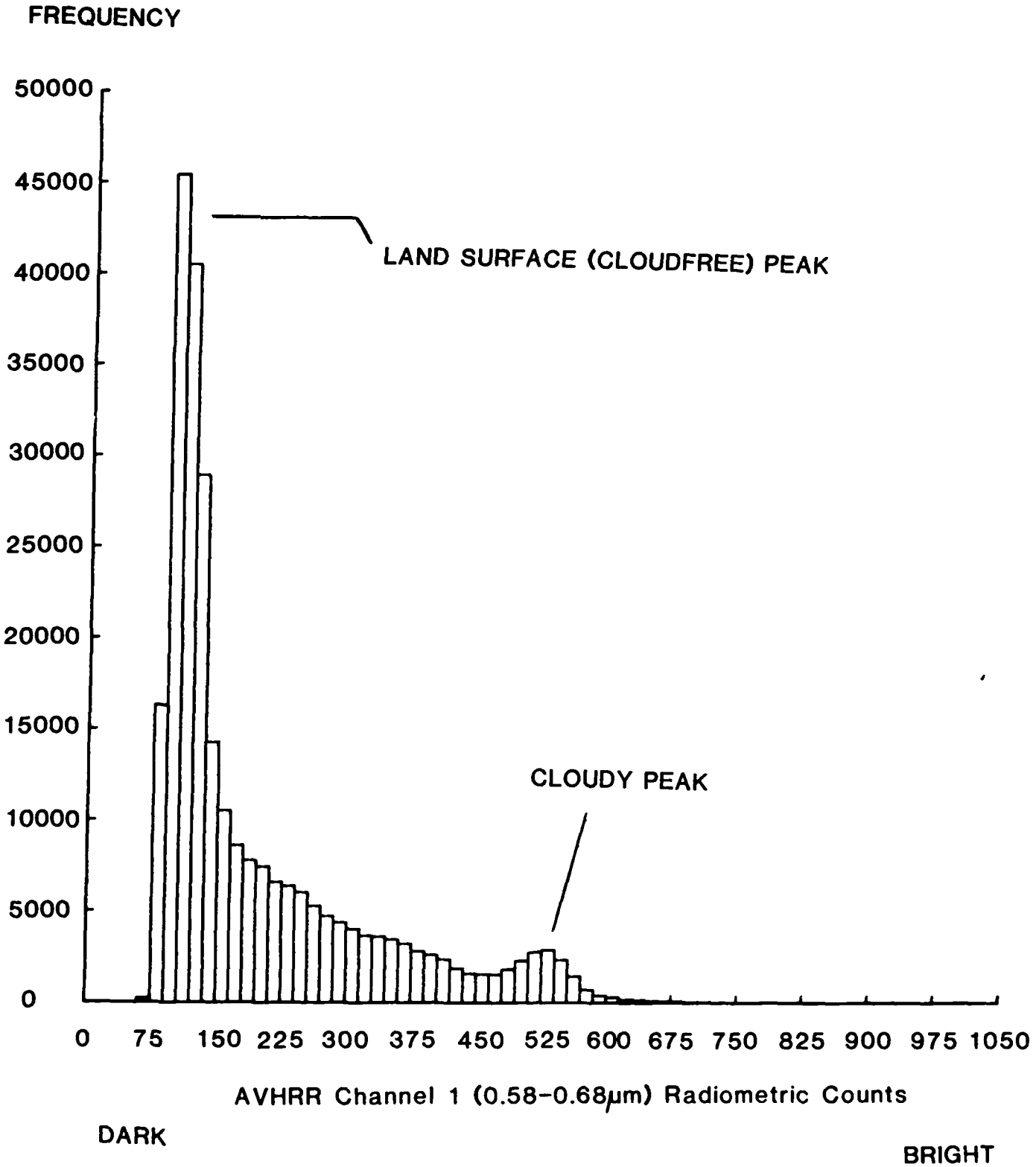

Figure 5(a) One dimensional frequency histogram for AVHRR channel 1 (0.58 - 0.68 μm) taken from a sub-scene, frame B (47° -52°) of Figure 1(a).

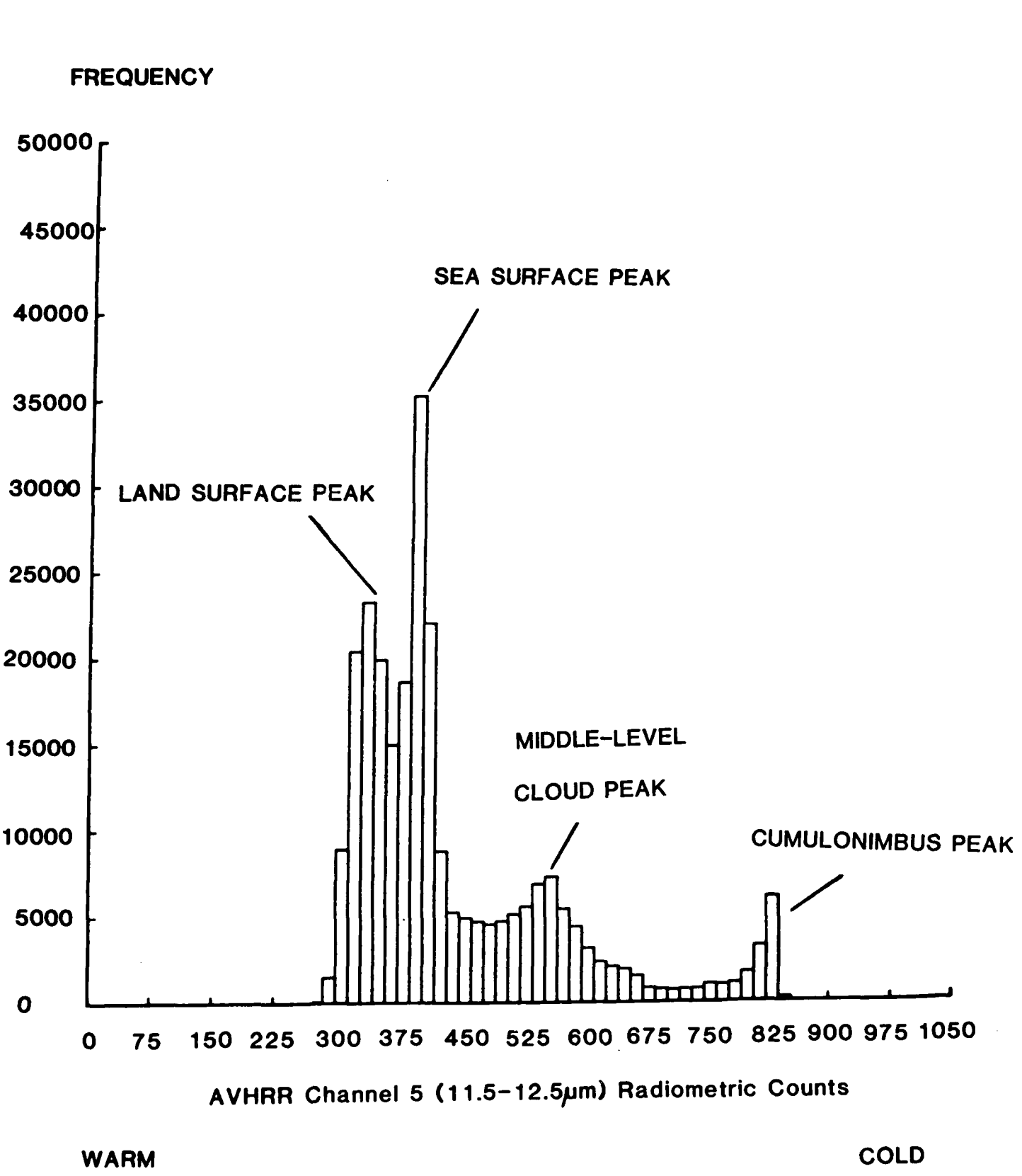

Figure 5(b) As for (a) but for AVHRR channel 5 (11.5 - 12.5 μm).

close proximity of the cloud free and cloudy peaks means that small changes in m,n and T will produce larger fluctuations in the derived cloud fraction. The latter case for spatial variations assumes that areas larger than the pixel resolution possess homogeneous surface properties and are never completely cloud-covered. The retrieval technique is therefore limited by surface variation over areas larger than an average cloud size which may be as large as 250 km x 250 km. One inherent problem with this method is that it does not offer a method of identifying apparent cloud variations resulting from variations in viewing geometry or atmospheric conditions.

The major drawbacks concerning the operational use of threshold algorithms relate to situations of partially clouded pixels and the definition of the clear sky radiance values. The problem of small clouds failing to fill up individual fields of view has been addressed (Coakley and Bretherton, 1982; Rossow et al., 1985) and might well apply in the case of, say, fair weather cumulus (Wielicki and Welch, 1986). If a threshold is selected to counter errors in mean cloud cover fraction for one cloud type, considerable biases may well then arise for other cloud types (Coakley and Bretherton, 1982). In addition, when only part of the field of view is covered, cold, thick clouds will appear warmer and thinner whilst warm, thin clouds might, in an extreme case, appear as a clear view to the surface thus introducing serious errors in determination of cloud amount, cloud optical properties and cloud top temperature. Coakley and Bretherton (1982) apply the findings of Shenk and Salomonson (1972) to highlight the risks associated with thresholds when the satellite's field of view is smaller than the typical cloud size by as much as two orders of magnitude. Plotting cloud cover errors against the inverse square

root of cloud area to scanning pixel size yields an approximate linear relation showing that the errors decrease inversely with the square root of cloud area (and hence cloud perimeter) thus explaining the likelihood of large threshold-based estimation errors for relatively small cloud size distributions.

The logical step to offset errors due to partial pixel coverage is to reduce the pixel resolution as far as possible, thus increasing the likelihood of completely clear or cloudy pixels. Unfortunately for global analysis pixel resolution is stringently controlled by the volume of resulting data so that whilst the Landsat thematic mapper (TM) has a resolution of 30 m and the Landsat multispectral scanner (MSS) a resolution of 57 m, as opposed to NOAA's advanced very high resolution radiometer's (AVHRR) value of 1.1 km, ISCCP will process only geostationary and AVHRR data which, will in turn, require subsequent compression. Ultimately, the accuracy of cloud cover determination rests with the success of the threshold technique in partitioning partially cloudy and clear pixels which in turn depends on the magnitude of the threshold (assuming clear sky radiances are known accurately) and on the methodology used to apply it.

The determination of clear sky radiances requires that at sometime during the time period examined, cloud free conditions prevail over each pixel. Providing that surface and atmospheric properties remain constant throughout the time period, the distributions of h_s and T_s over the pixels may be accurately obtained and the clouds become discernible through a single spectral channel. However, sudden or gradual spatial and/or temporal variations in the surface or atmospheric properties such as a heavy fresh snowfall or an

increase in atmospheric turbidity due to an influx of desert aerosol can render the clear sky radiances inaccurate. For example Rossow et al., (1985) describe such a sequence of events that occurred during the ISCCP pilot study test period. Assuming reliable clear sky values the use of small thresholds can allow for the detection of clouds whose spectral signatures closely resemble that of a clear sky, e.g. low level clouds detected by use of a discriminating visible channel threshold (Saunders 1986).

The presence throughout the world of spatial inhomogeneity and temporal variation of the surface, means that the use of fixed thresholds for analysis of global radiance data is completely impractical. Thresholds would have to be 'tuned' to the situation in hand using auxiliary data. Not surprisingly, one of the major findings of the ISCCP pilot study was the urgent need for improvement in the techniques to specify clear sky radiances. Future improvements in satellite cloud retrieval are likely to arise directly as a result of a superior determination of the clear sky scene.

Application

Despite the attendant problems outlined above, threshold-based cloud retrieval techniques have been successfully used in several instances (Liljas 1984; Minnis and Harrison, 1984a,b,c; Saunders 1986). The accurate determination of sea surface temperature via remote sensing may be used as data input to climate and forecast models. Conventional sounding techniques rely on cloud free conditions for operation which, during periods of persistent scattered or total cover may be an unacceptably long time in forthcoming. The dynamic visible threshold method (Saunders 1986) has been successfully utilised in daytime hours as a component of a larger algorithm known

as the spatial coherence visible method to provide accurate sea surface temperature values by comparison with ship measurements. Here a fixed threshold (the gross cloud check) immediately rejects obviously cloudy pixels whilst the dynamic threshold, operated in combination with the spatial coherence method (see Section 2.3) distinguishes sea surface from low cloud whilst remaining unaffected by any strong sea surface temperature gradients in the vicinity of frontal regions.

In attempting to estimate diurnal variations of cloudiness in association with clear sky parameters, the 'hybrid bispectral' threshold technique (Minnis and Harrison, 1984a,b,c) has been introduced and applied to subregions of GOES-East images. At night the method reduces to a simple infrared threshold but the daytime visible radiances are employed to tune the night-time threshold and thus the consistency is preserved throughout the diurnal cycle (Minnis and Harrison 1984a). The clear sky visible reflectances are obtained from time records of minimum reflectance for observations at a time close to midday, R then being assumed constant throughout the time period. Empirically derived reflectance models which take account of surface properties, solar zenith angle and the satellite viewing geometry enable determination of R_S at other times. Average values of R_S for each subregion of 250 km x 250 km are obtained with ΔR set at approximately 1% reflectance. The brightness temperature threshold is then determined by summing (for decreasing values of T) all the pixels for which $R<R_S + \Delta R$ until their average value is equal to $\bar{T}$, the average of all the pixels where $R<R_S + \Delta R$. The final value of T used in the summation defines $T_S - \Delta T$ and all pixels colder than this

value are labelled cloudy (irrespective of reflectance). In this way despite the inclusion of slightly cloudy pixels or those containing cirrus cloud (poorly detected by visible thresholds) which may cause $\bar{T} < T_s$ the effect of counting partially cloudy pixels as totally cloud is offset. In the next stage all R_s, R and T values are normalised, thus removing any angular dependence or atmospheric effects. Empirical reflectance models for land, cloud, ocean and a clear atmosphere are applied to the reflectances to normalise them with respect to the solar zenith angle, the satellite viewing zenith angle and the satellite viewing azimuth angle, whilst application of seasonal and latitude-dependent limb darkening functions helps eliminate any water vapour absorption effects from the T values by normalising to the overhead satellite-viewing zenith angle of zero degrees and thus correcting for slanted paths, reducing the amount of atmospheric attenuation possible by water vapour absorption, (Minnis and Harrison 1984a). The clear pixels permit surface temperature, averaged over a subregion to be estimated, and the cloud optical properties are deduced from R, T, R_s, T_s and f, for each pixel. These properties can be assigned to a low, middle or high cloud category by defining, for each category, a range of temperatures interpolated from T_s assuming a uniform lapse rate. The results of the Minnis and Harrison (1984a,b,c) application of the bispectral threshold to monthly GOES data could be compared with the monthly cloud distributions obtained from long term climatological values (e.g. Hahn et al., 1984) as a possible 'validation'.

The potential uses of automated cloud classification include climate modelling, numerical weather forecasting, solar energy utilisation and agricultural applications. The European Space

Operations Centre (ESOC) already operates such a procedure for mapping areal distributions of the cloud top level whilst the Swedish Space Corporation (SSC) employs an automated classification algorithm for use in forecasting, described by Liljas (1984). The method is known as multispectral box classification and makes use of four AVHRR channels (1, 2, 3 and 4; 0.58 - 0.69 μm, 0.73 - 1.10 μm, 3.55 - 3.93 μm, 10.5 - 11.5 μm) to examine the radiative properties of clouds and land, ocean and cryospheric surfaces as a function of their optical depth, height, density and thermodynamic phase. Liljas (1984) describes the spectral characteristics of each common cloud type for the channels used (Figure 6), and demonstrates how the spectral similarities between snow, mist, sunglint and clouds in channels 1 and 4 can be overcome by the use of channel 3 (Figure 7), where the application of channel 3 brightness temperature minus channel 4 brightness temperature, normalised by division by the sine of the solar elevation angle, E, provides a measure of the reflectance of solar radiation in channel 3 (Table 2) (Liljas, 1984). The implementation of fixed thresholds in the n-dimensional radiance intensity space (where n represents the number of spectral channels used) is used to define 'boxes' for 16 cloud and surface types (Table 3) for the summer period May to September. The method shows considerable agreement in comparison with synoptic surface observations, although a comparison with different (i.e. non-threshold) types of algorithm, whilst not yet attempted would prove a useful exercise. Unfortunately Liljas (1984) fails to provide information concerning the sensitivity of the applied thresholds to changes in season (and hence surface properties) although some level of tuning seems likely to be necessary. However, from the

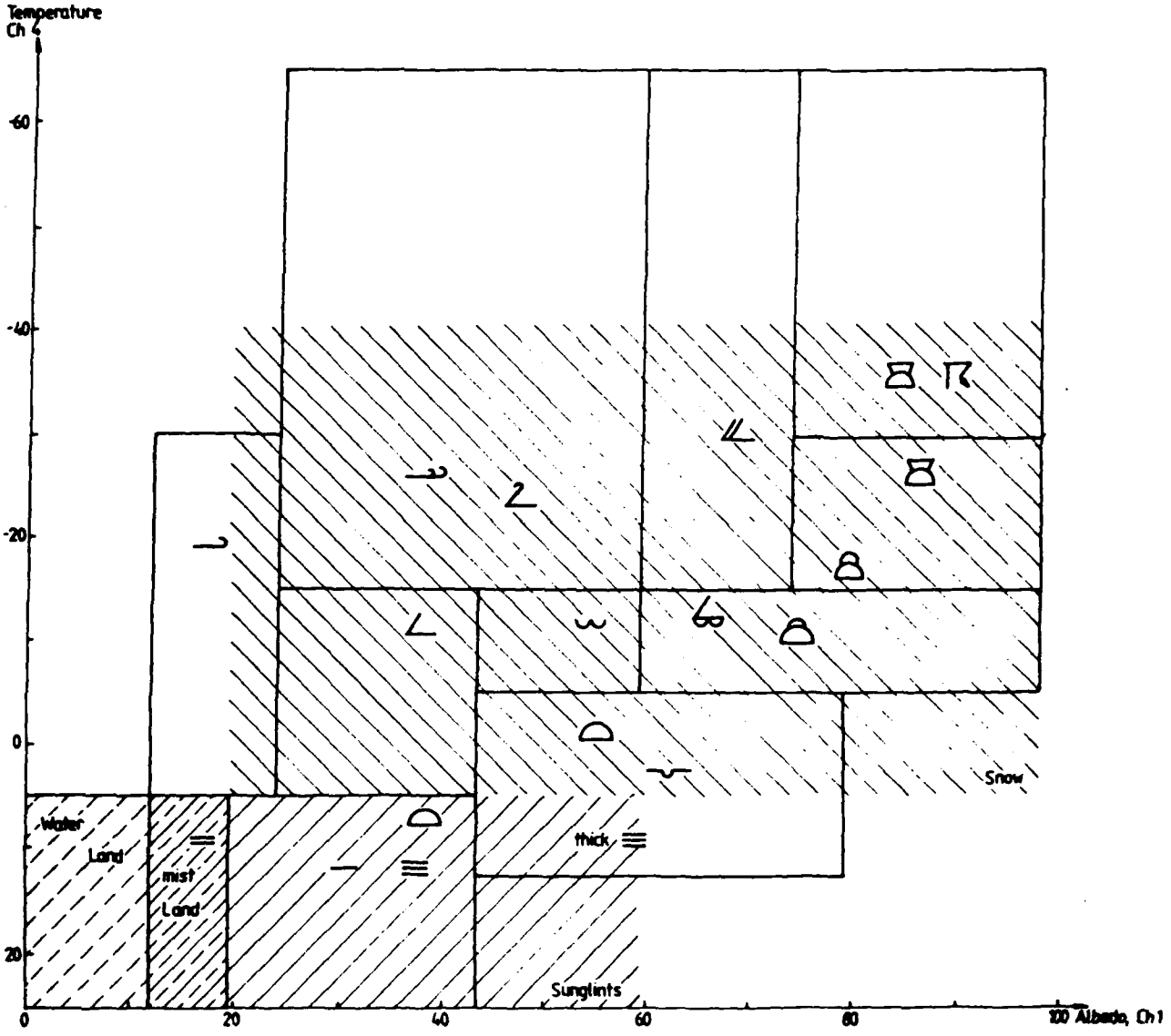

Figure 6 Position of various surfaces in visible (channel 1, 0.58 - 0.68 μm) and infrared (channel 4, 10.5 -11.5 μm) intensity space from AVHRR data (after Liljas, 1984). Standard U.K. Meteorological Office cloud symbols are used.

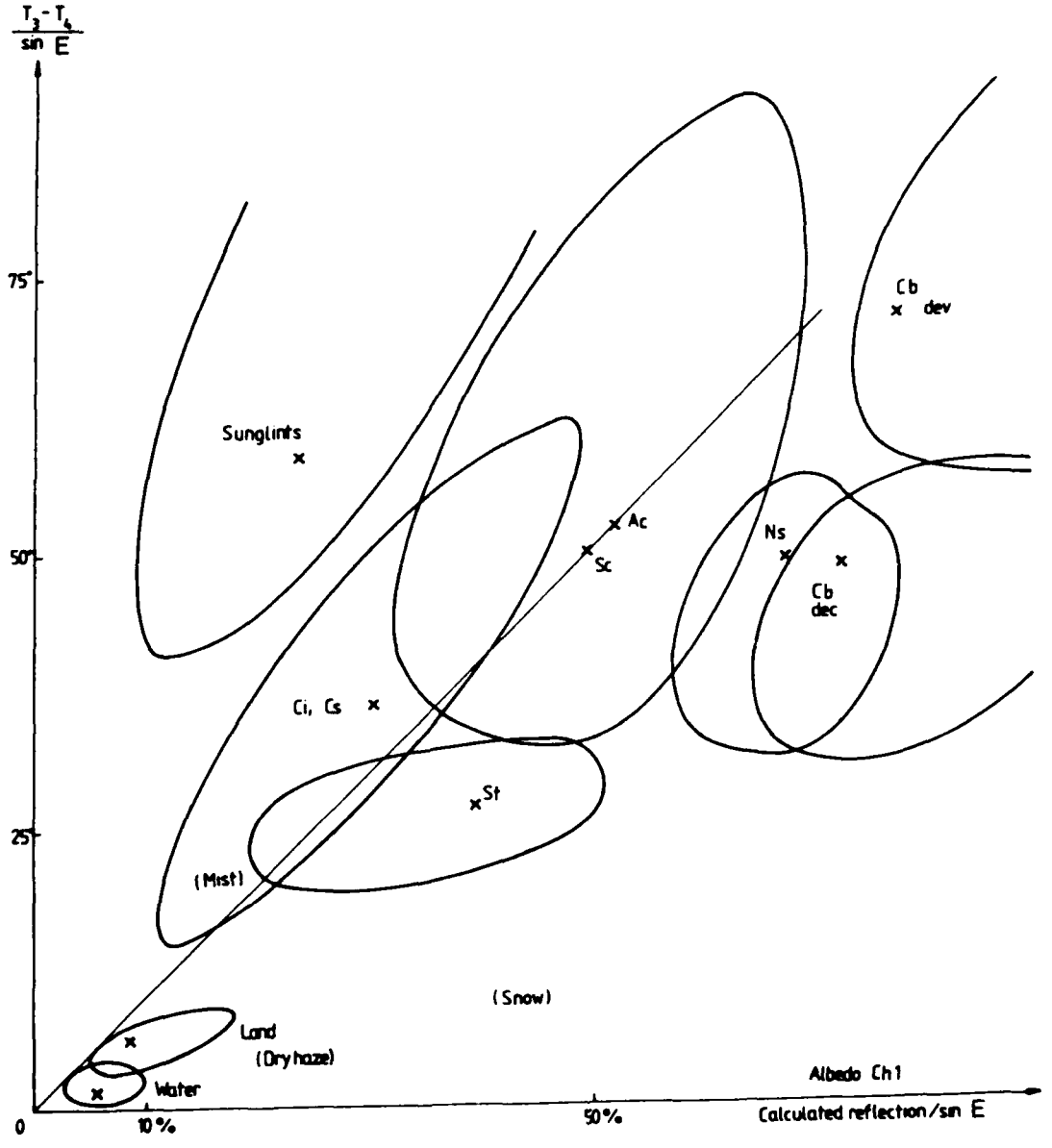

Figure 7 Positions of different reflecting surfaces in two-dimensional intensity space. The vertical axis is the brightness temperature difference (°C) in channels 3 (3.55 - 3.93 μm) and 4 (10.5 - 11.5 μm) normalised by division by the sine of the solar elevation angle, E, to an overhead sun value. The horizontal axis is the normalised cloud reflectance in channel 1 (0.58 - 0.68 μm) (after Liljas, 1984).

Table 2. Albedos for various terrestrial surfaces and cloud types calculated from AVHRR channel 1 and brightness temperature difference in AVHRR channels 3 and 4. Mean value and extremes for May to September of well defined surfaces (after Liljas, 1984).

Cloud / surface type	Albedo [extreme - mean - extreme]	$(T_3-T_4)/\sin E$ (°C) [extreme - mean - extreme]
Thin stratus/fog	0.20-0.40-0.52	20-27-36
Stratocumulus *	0.40-0.50-0.60	32-50-69
Altocumulus	0.37-0.50-0.69	33-52-90
Nimbostratus	0.59-0.68-0.77	31-49-62
Cirrus/cirrostratus	0.12-0.31-0.62	14-36-62
Cumulonimbus developing or mature	0.75-0.78-0.92	62-71-85
Cumulonimbus decaying	0.66-0.73-0.92	30-49-61
Sunglints	0.10-0.24-0.40	-58-
Water	0.03-0.06-0.01	0.2-1.5-4.5
Land	0.05-0.09-0.18	2.5-5.8-8.0

Notes

Between 10 and 40 studied objects in every class
Sun elevation angle, E, between 30 and 55 degrees

* seven to eight oktas (eighths) of sky cover

Table 3. The separation of sixteen classes in a four-dimensional intensity space (maximum and minimum values) for NOAA-6 imagery for solar elevation angles of between 41° and 47° (after Liljas, 1984).

Cloud/surface	Ch 1	Ch 2	Ch 3	Ch 4
Cb	132-172	100-150	101-255	163-255
Cb	132-172	100-150	101-255	160-182
Ns	106-131	80-130	101-255	160-255
Cs	48-105	30-90	101-255	160-255
Ci over water	24-47	15-30	101-255	121-182
Ci over land	24-47	31-50	101-255	121-182
Cu congestus	106-172	80-150	101-255	140-159
As	48-80	30-80	101-255	121-159
Ac	81-105	65-100	101-255	140-159
Sc	81-131	65-120	101-255	100-139
Mist over land	27-40	38-60	101-255	60-120
Mist over water	24-40	22-37	101-255	60-120
St/fog	41-80	30-80	101-255	60-120
Water	0-23	0-20	101-255	60-120
Land	0-26	21-60	101-255	60-120
Sunglints	10-100	10-100	0-100	60-120

examples given the diagnostic value of the classification in real-time meteorological analysis and forecasting appears to be high.

2.2 Statistical Cloud Retrieval

In either clear sky, single cloud type or multicloud type situations, projection of the multispectral signature of each satellite image pixel onto a corresponding multi-dimensional histogram will give rise to the presence of areas of relatively high pixel density. These regions, dispersed throughout the radiance intensity space are associated with relatively homogeneous emitting and reflecting surfaces, cloud types, oceans and land. The ability to describe and to discriminate effectively between these surfaces or classes, essential for any meaningful cloud classification scheme, has prompted the invocation of statistically-based retrieval algorithms which, as opposed to the threshold methods, are designed to treat large groups of pixels at a time, corresponding to each surface type. The methodology employed in separating spatial radiance patterns into cloudy and clear classes can be thought of as being equivalent to the use of a constant threshold and clear sky radiance. For complex cases this would appear to be an unattractive concept, however as will be seen, use of time compositing can be beneficial for statistical algorithms as well.

The fundamental philosophy of statistical cloud analysis is the partitioning of multidimensional frequency histograms into representative classes for which three recognised routes exist. These are (i) gaussian histogram analysis (Simmer et al., 1982; Phulpin et al., 1983); (ii) dynamic clustering (Desbois et al., 1982); (iii) spatial coherence method (Coakley and Bretherton, 1982; Coakley, 1983; Coakley and Baldwin, 1984). As the different method descriptions use

the terms "class" and "cluster" synonymously and interchangeably, this convention will also be adopted here.

2.2.1 Gaussian Histogram Analysis

Simmer et al., (1982) along with Phulpin et al., (1983) present examples of histogram partition by way of fitting Gaussian (normal) distribution functions to one and two-dimensional frequency histograms in order to isolate distinct clusters. At the time of publication the latter method had only been developed and tested for cloud layers overlying oceanic regions, although the intention was to develop a similar technique for use over land surfaces. The asymmetric Gaussian analysis of Simmer et al.,(1982) does not suffer from this limitation. Neither method at present takes account of corrections for viewing geometry or atmospheric effects. Implicitly built into these analyses is the radiative model in which, as previously stated, different surfaces can be represented as peaks in the histograms by virtue of their homogeneity and consist of clusters of distinct radiance pairs.

In Phulpin et al., (1983) the AVHRR data array was first divided up according to the operational grid for the Tiros operational vertical sounder (TOVS). This was because the work was carried out in the context of improving vertical temperature profiles in cloudy areas. The data are subsequently calibrated and the visible one-dimensional and two-dimensional histograms constructed. Gaussian functions with fixed standard deviations are fitted to the histogram peaks to identify distinct sea and cloud clusters which must contain at least a threshold minimum number of pixels. Closely adjacent peaks are taken to represent the same layer and are merged into one class, following a pre-defined set of rules. Cloud cover estimation is by

summing up all the pixels in the cloudy clusters and dividing by the total number of array pixels.

Validation

Validation would consist of comparison with visually interpreted enhanced images by experienced cloud analysts, identifying the clouds by their texture and spectral features. They are reckoned to be able to estimate total cloud amount to within an accuracy of 10%. Combinations of data from channels 1 (0.56 - 0.68 μm) and 4 (10.5 - 11.5 μm), along with 2 (0.73 - 1.10 μm) and 4 were used in construction of the histograms with the result that the near infrared channel 2 proved significantly better than channel 1 for cloud analysis, mainly due to the lower reflectance of the sea, thus allowing for better spectral resolution of cloud free regions (see Figure 8). Altogether almost 90% of the cases were in close agreement with the visual interpretations, with the most persistent difficulties arising in the discrimination between small, low-level cumulus and the sea surface, a problem akin to that caused by boundary layer cumulus in the threshold method. The potential role of channel 3 (3.55 - 3.93 μm), although considered, is as yet unresolved.

The idea developed by Simmer et al., (1982) is that peaks appearing in one-dimensional histograms (both visible and infrared) can be represented by Gaussian functions which can, in turn, define clusters in two-dimensional radiance space. The standard deviations of the Gaussian curves are determined from the plot of radiance versus the logarithm of infrared frequency and the first cluster's pixels redefined on the basis of distance from the peak radiance. This process is carried out first for the infrared histogram and subsequently, whilst only using the pixels assigned to the first

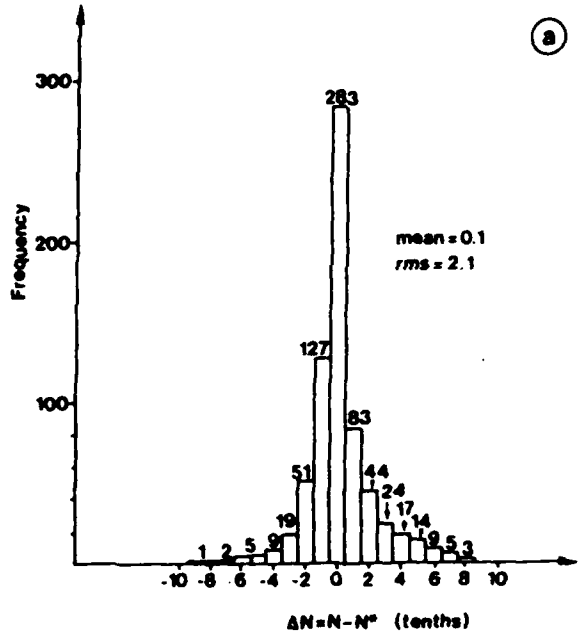

Figure 8(a) One dimensional frequency histogram of $\Delta N = N - N^*$ constructed from AVHRR data (channels 1, 0.,58 - 0.68 μm and 4, 10.5 - 11.5 μm) for Europe and the Atlantic Ocean where N represents the cloud cover computed from the retrieval algorithm and N^* is the value derived from visual nephanalysis (after Phulpin et al., 1983).

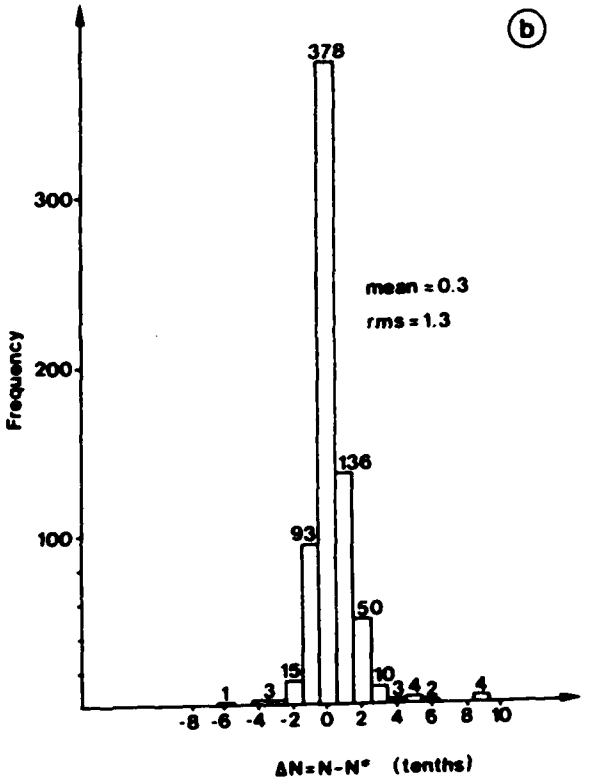

Figure 8(b) As for (a) except for AVHRR channels 2 (0.73 -1.10 μm) and 4 (10.5 -11.5 μm) (all after Phulpin et al., 1983)

cluster, on the visible histogram so as to define the first two-dimensional cluster. The whole process is repeated until either all image pixels are assigned to a cluster or a set number of clusters have been defined, any remaining pixels being assigned to the nearest (in two-dimensional space) cluster. Cloud cover fraction is estimated as in Phulpin et al. (1983) whilst surface and cloud properties are calculated from the mean radiance over a particular cluster for pixels residing within a radius of one standard deviation of the peak frequency. Stable statistics can be achieved by operating on a subregion of at least 300 image pixels.

This latter method was included amongst those tested in the ISCCP pilot study. Its degree of success was judged to be dependent upon the decision criteria and the resulting effectiveness of the cluster definition. It performed to around the same level as the bispectral threshold but encountered problems in regions of high spatial inhomogeneity and in the case of a time-varying surface.

2.2.2 Dynamic Clustering

A significant aspect of any cloud retrieval is that it is carried out in the most objective manner possible. The examples so far have involved tasks such as threshold tuning and the use of visual image interpretation which invoke a degree of subjectivity. Correspondingly the most objective cluster definition should give rise to the most objective statistical method. The dynamic cluster algorithm (Desbois et al., 1982; Desbois and Sèze, 1984a) has an essentially objective framework and has been modified several times over various cloud distributions. The step by step procedure of cluster selection can be found in Desbois et al., (1982). Here, the method is discussed in the

overall context of classification (Desbois and Seze, 1984a,b and Seze et al., 1984).

The statistical requirements of the technique involve the use of several thousand pixels (termed the learning set) in a test run. These may or may not represent the image pixels on which the classification will be performed. One, two or three-dimensional histograms are then constructed from the learning set. As opposed to Gaussian techniques, those that have clusters classified from METEOSAT imagery (as in Desbois et al., 1982) use the available water vapour channel (5.7 - 7.1 μm)in addition to the visible (0.4 - 1.1 μm) and infrared (10.5 - 12.5 μm), resulting in the use of three instead of two-dimensional histograms. Correct alignment of the image channels is needed because the position of every pixel in the various histograms will determine its class. Application of the dynamic cluster method to the histograms now follows, either from randomly selected pixel groups (kernels) or from pre-designated kernels. Although at times useful, the pre-designated kernels are to be avoided if the classification is to remain wholly objective. The end product of the procedure is firstly, the number of classes separated, secondly their centres of gravity and variances, and finally the percentage of pixels from the learning set in each class. Classification of the image under study is achieved by assigning each pixel to the class it lies closest to, the distance to a class referring to the sum of the variance of the class and the Euclidian separation between the image pixel and the centre of gravity of a class.

Visual examination of the histograms allows a qualitative assessment of the cloud systems present to be made and in simple cases the classes can be identified directly from the histograms. Examples

of one and two-dimensional histograms, similar to those given in Desbois et al. (1982) have been derived from NOAA-7 AVHRR data depicted in Figure 1. The one-dimensional histograms (Figures 9-12) illustrate peaks of varying intensity and definition, the visible (channel 1) data tending to be more smoothed than the infrared (channel 5), resulting in easier class recognition in the latter. The separation of the three major classes present in the sub-scene termed here frame A [52^{o} - 57^{o}] (Figures 9 and 10), (land surface, sea surface and low stratocumulus) is more easily performed on the infrared histogram. Likewise the sub-scene termed frame C [42^{o} - 47^{o}] (Figures 11 and 12), the very broad peak lying adjacent to the land surface peak contains both middle and high level convective clouds which can only be distinguished on the infrared histogram. The corresponding (Figures 13 and 15) two-dimensional histograms are shown along with the corresponding results for the sub-scene termed frame B [47^{o} - 52^{o}] in Figure 14. Once again several classes are immediately identifiable by their positions in the radiance intensity space whilst those less obvious would subsequently be deduced from dynamic clustering. Broader peaks in the one-dimensional histograms express themselves as areas contained within but which are themselves devoid of contours in two-dimensions. Projection of the two-dimensional plots onto a three-dimensional surface (Figure 16) provides an additional aid to visual class separation.

The major drawbacks concern occasions when the histograms fail to show definite peaks but instead tail off gradually from a single, ill-defined peak (Wielicki and Welch, 1986). In such a case the algorithm, whilst still separating classes, fails to draw sharp boundaries between

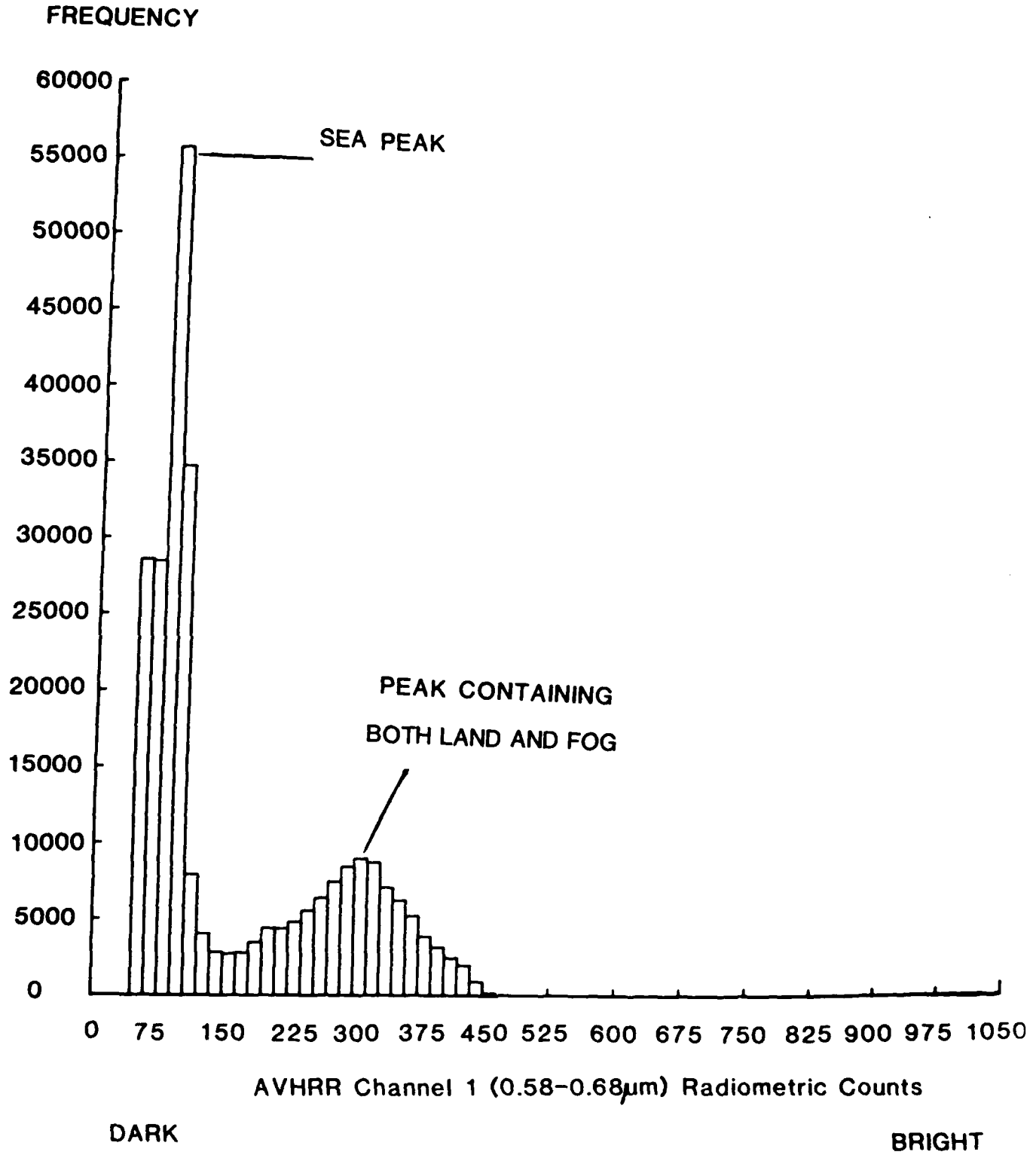

Figure 9 One dimensional frequency histogram for the AVHRR visible channel 1, (0.58 - 0.68 μm) for sub-scene, frame A (52^{o} - 57^{o}) of data shown in Figure 1.

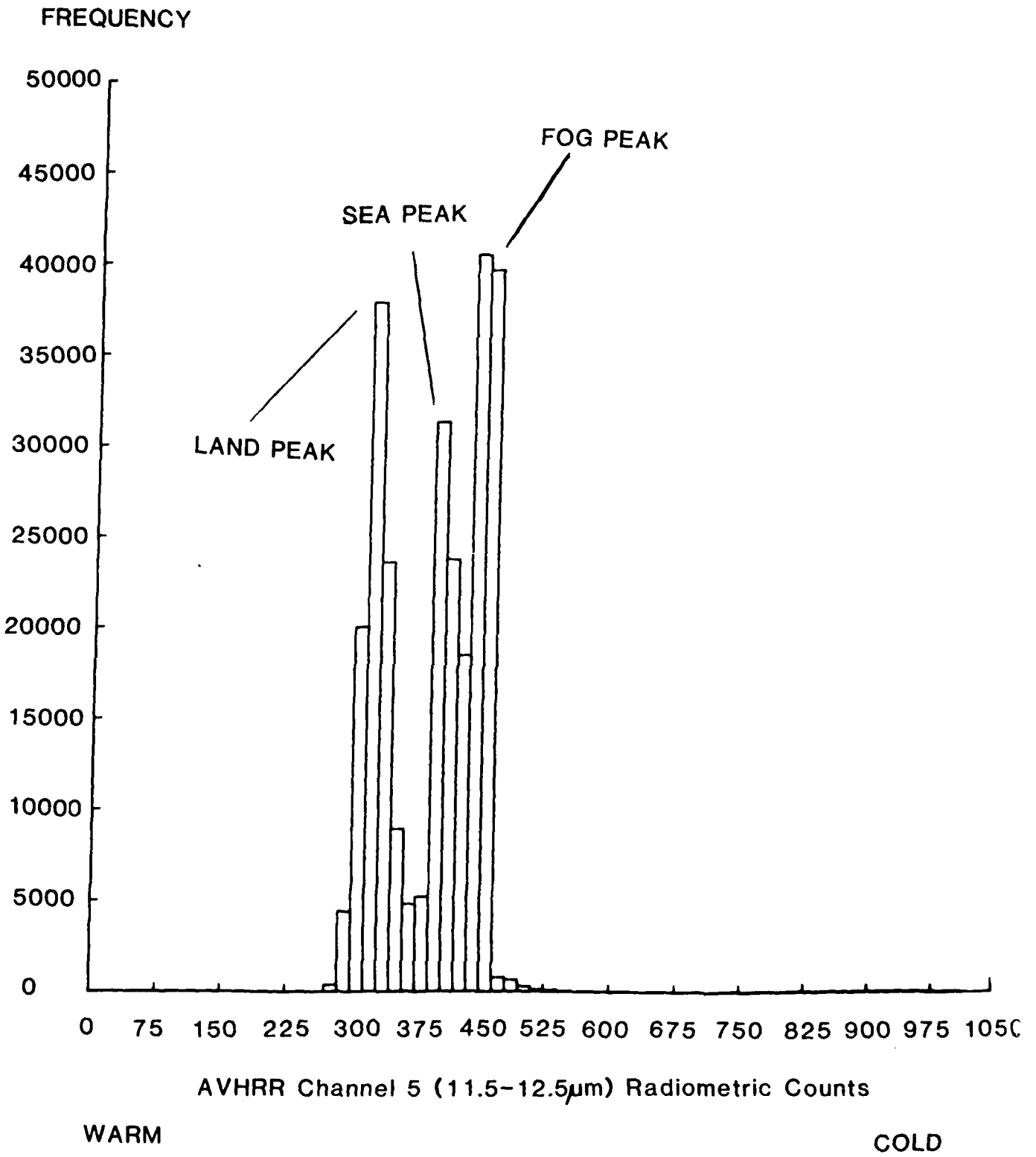

Figure 10 One-dimensional frequency histogram for the infrared AVHRR channel 5 (11.5 - 12.5 μm) for sub-scene, frame A (52° -57°) of data shown in Figure 1.

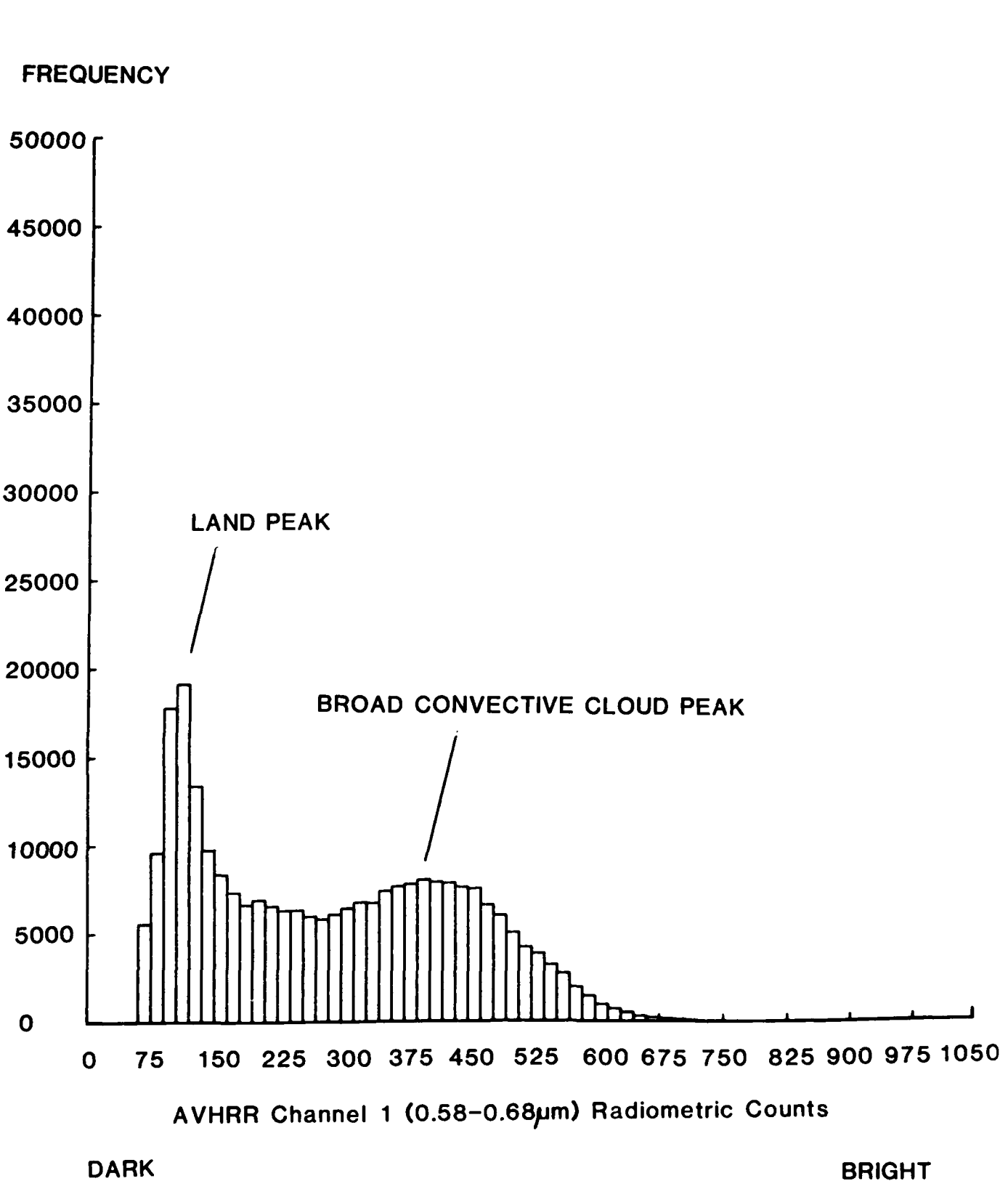

Figure 11 One-dimensional frequency histogram for the visible AVHRR channel 1 (0.58 - 0.68 μm) for sub-scene, frame C (42° -47°) of data shown in Figure 1.

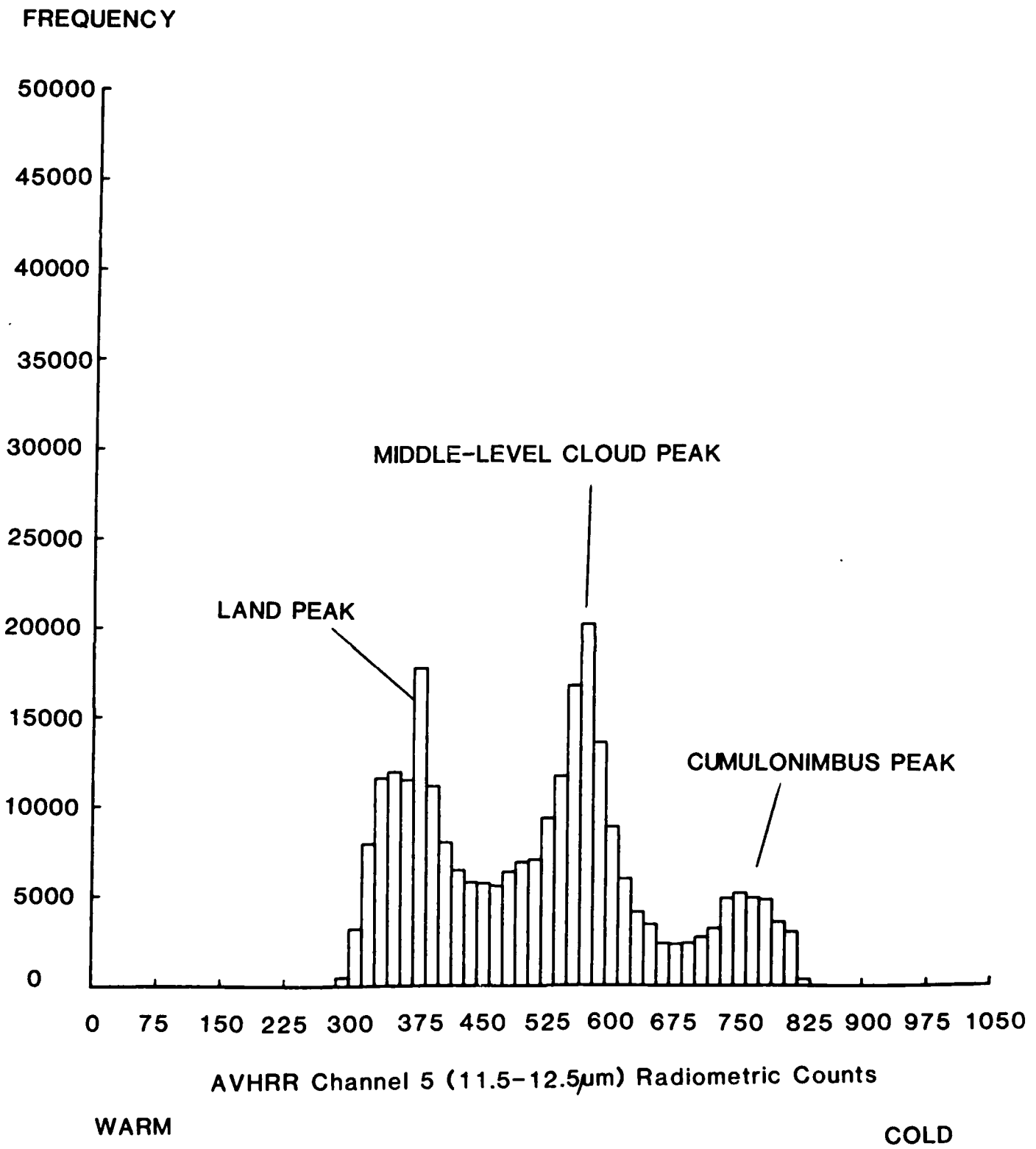

Figure 12 One-dimensional frequency histogram for the infrared AVHRR channel 5 (11.5 - 12.5 μm) for sub-scene, frame C (42° - 47°) of data shown in Figure 1.

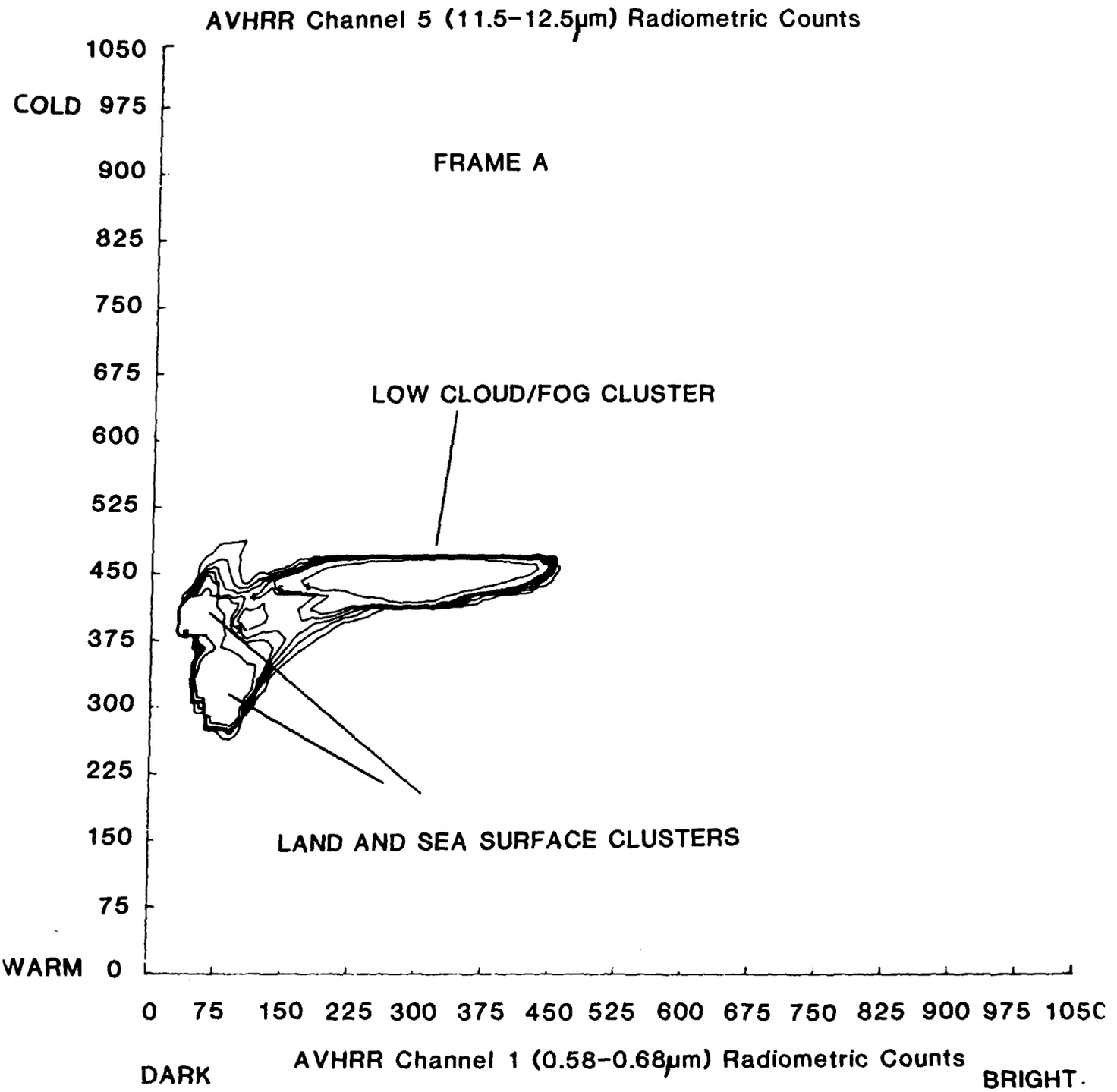

Figure 13 Infrared/visible (AVHRR channels 1, 0.58 - 0.68 μm and 5, 11.5 -12.5 μm) bidimensional histogram for sub-scene, frame A (52° - 57°) of data shown in Figure 1.

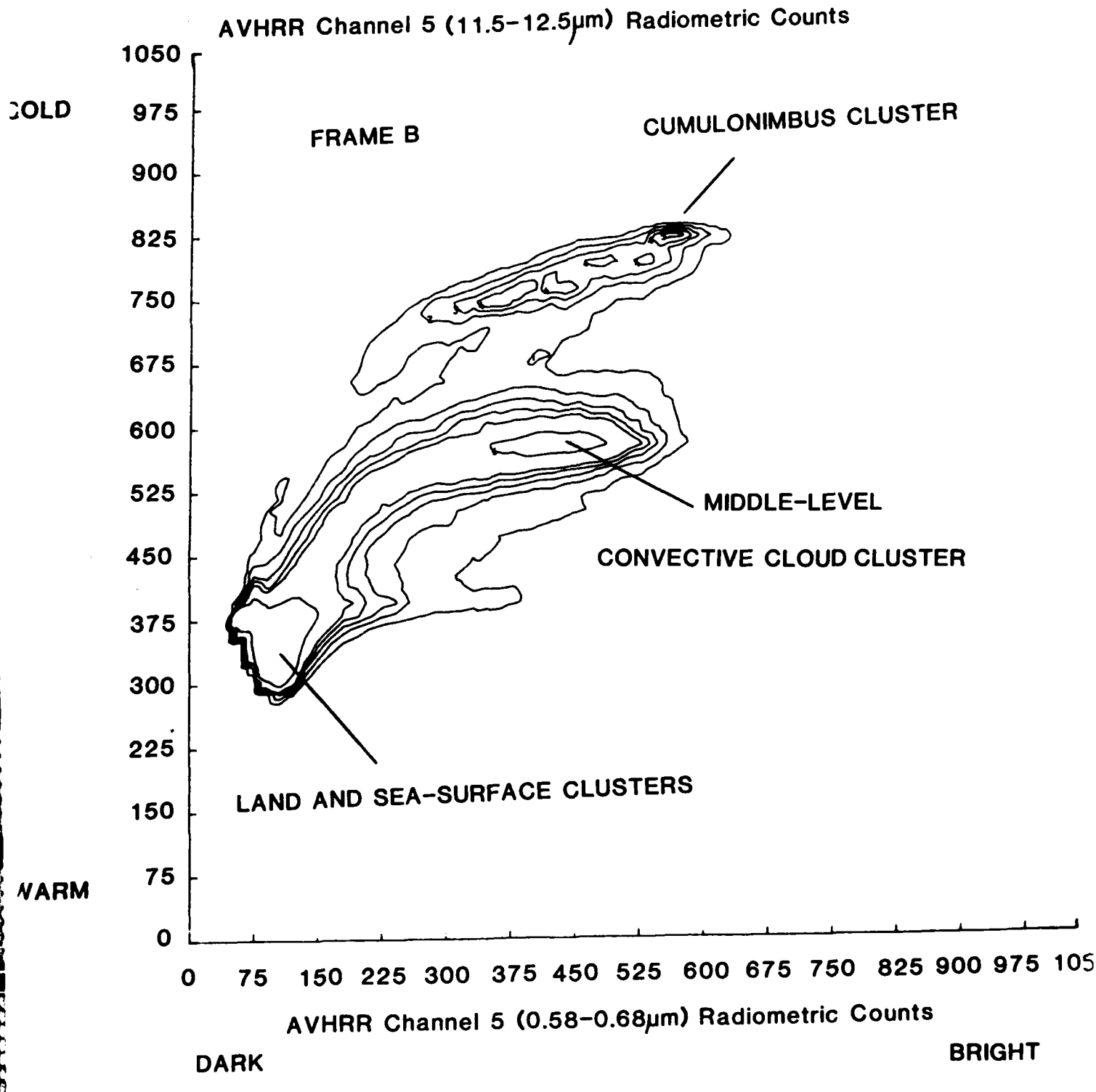

Figure 14 Infrared/visible (channels 1, 0.58 - 0.68 μm and 5, 11.5 - 12.5 μm) bidimensional histogram for sub-scene, frame B (47^{o} - 52^{o}) of data shown in Figure 1.

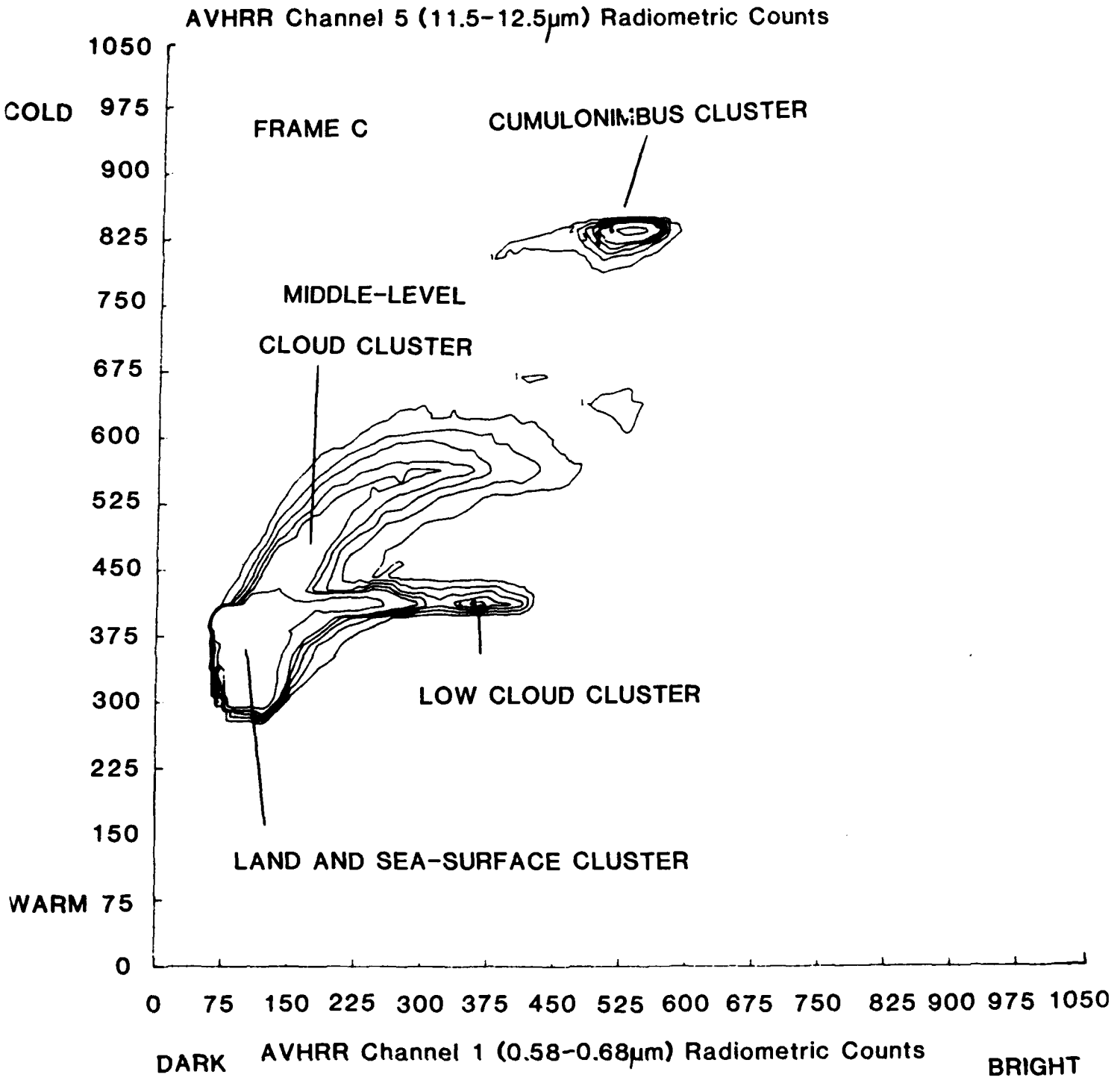

Figure 15 Infrared/visible (channels 1, 0.58 - 0.68 μm and 5, 11.5 - 12.5 μm) bidimensional histogram for sub-scene, frame C (42° - 47°) of data shown in Figure 1.

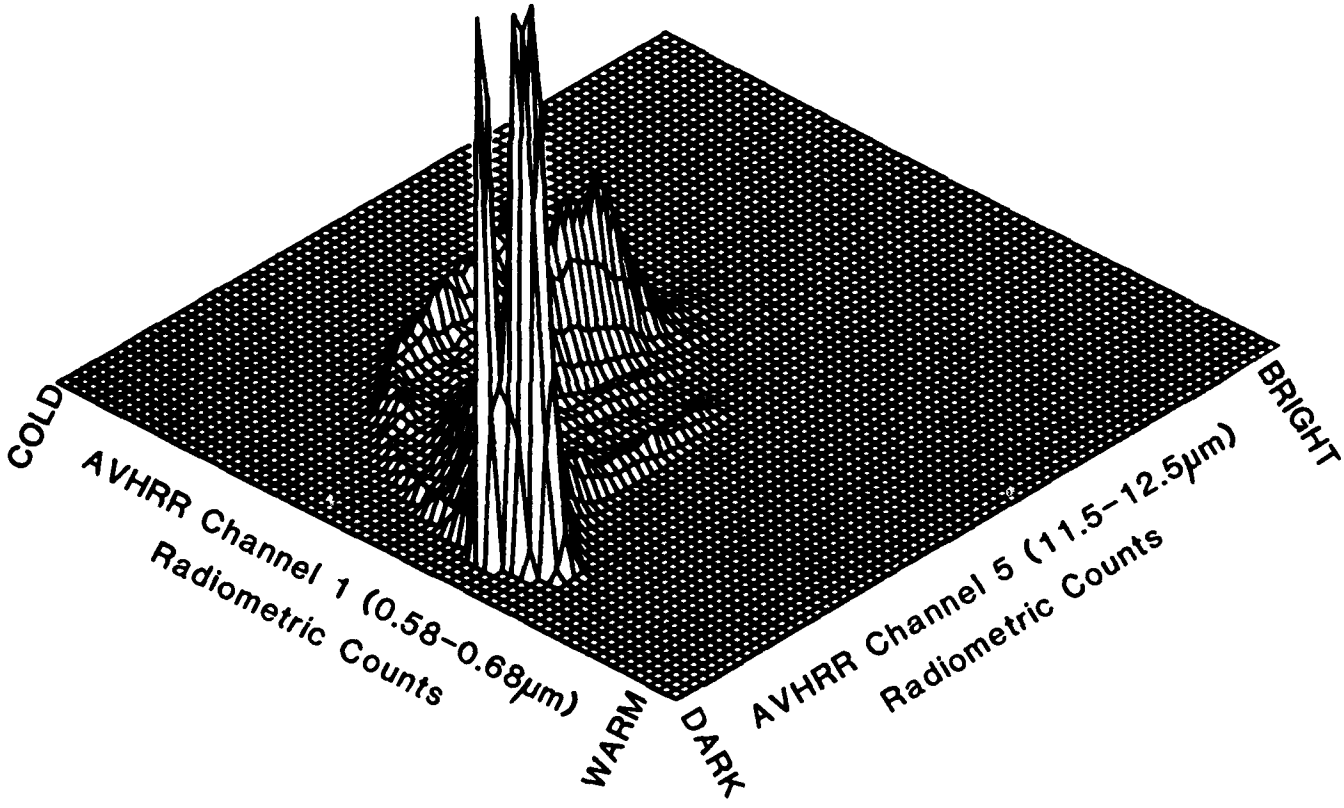

Figure 16 Projection of Figure 14 on to a three-dimensional surface.

neighbouring classes. This effect was noted in the ISCCP pilot study (Rossow et al., 1985) and would produce analogous problems in the Gaussian analyses (Section 2.2.1). Secondly the dynamic cluster method requires initial choices of the number of classes and the number of points in each kernel. These values can have a profound effect upon the number of final classes that result which is generally too large.

Application

Application of this type of cloud classification to individual image segments carries with it the inherent risk that adjacent segments might not produce equivalent classes, depending on the cloud amount and distribution. The same can be said of the same image segment examined at various time intervals. Should this occur it would make larger scale classification extremely difficult. One solution to this problem is to begin with learning sets of a sufficient size so as to exceed the minimum number of points required for a representative cloud population and statistical stability. In this way the classes found at larger scales can be reproduced at smaller scales. Alternatively time sampling can be used whereby the learning set is derived from time series of an image segment, each image taken at the same time each day for several successive days. The resulting cumulative histograms are then likely to contain distributions of most types of cloud and surface. An interesting feature of this sampling would be the large number of partially cloudy pixels spread out through the histograms, as would be those pixels depicting semitransparent cloud.

The original method was tested on METEOSAT images over the tropical Atlantic, central and West Africa (Desbois et al., 1982). Although no corrections for atmospheric effects or viewing geometry were made, the close proximity of the study region to the equator

reduced the likelihood of the latter type of error. Individual image segments used for the initial testing for statistical stability included 6000 pixels and the subsequent full study involved 40,000 pixels. The analysis centered on an area of convective disturbances proviaing a varied class distribution. The retrieval produced up to 6 different classes (see Figures 17 and 18 and Table 4) which were identified by referring to the three two-dimensional histograms and the rectified images. The classes were found to correspond well with the cloud types present, encouragingly discriminating the presence of cirrus.

In addition to classification Desbois et al., (1982) demonstrate a method of determining semitransparent cloud top temperature from the infrared/water vapour histogram. Results were encouraging and could possibly be used as correlative data in future applications of other retrieval algorithms.

Methods for Improving Classification

Since the original testing of the dynamic clustering technique reported in 1982, much effort has been devoted to finding means of achieving greater representation in the cloud classes. Some new ideas have since emerged: (i) use of space and time sampling to obtain a fuller representation of the cloud distribution (discussed in the previous section) (Desbois and Séze, 1984a) and (ii) comparison of local spatial variances to separate the more homogeneous cloud clusters (Séze and Desbois 1986). One of the objectives of Desbois and Séze(1984a,b), was to perform a modified retrieval using the recommendations above and to compare the results with those derived from thresholds. The first modification is that of deriving the

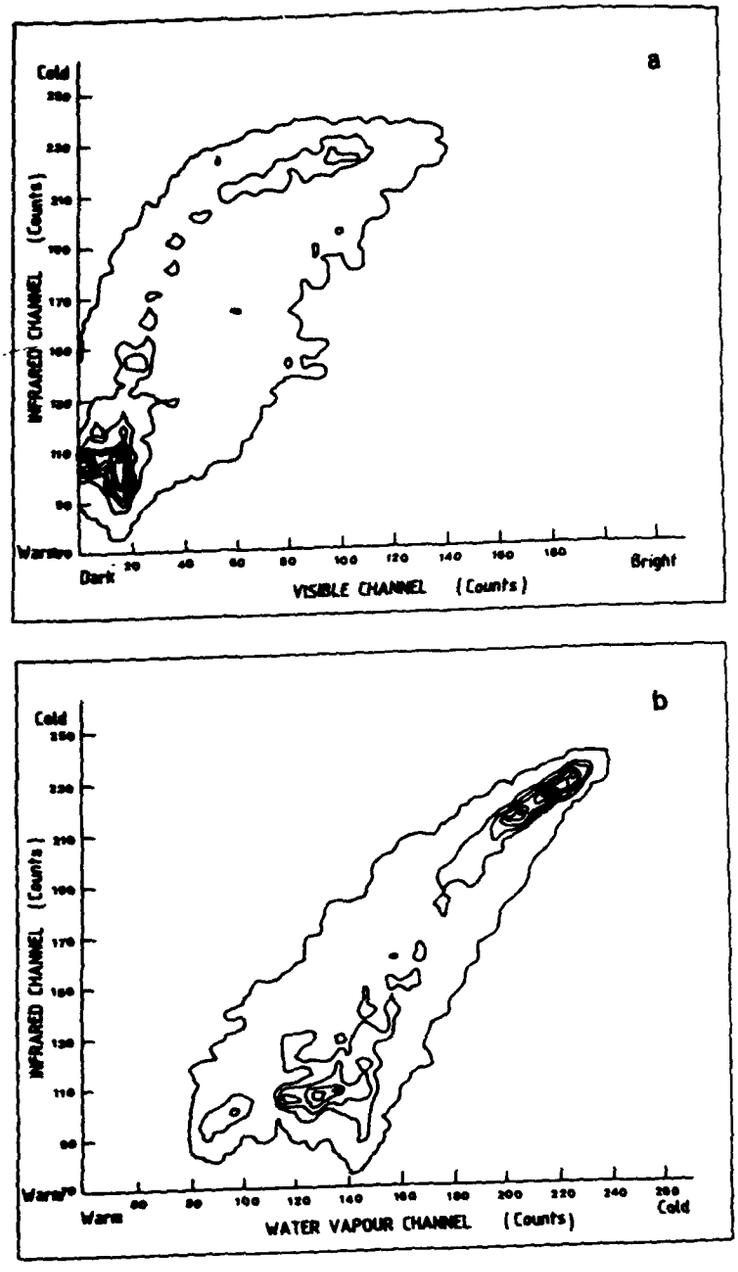

Figure 17 Bidimensional histograms for an analysis region, IR-VIS, IR-WV and VIS-WV (after Desbois et al., 1982).

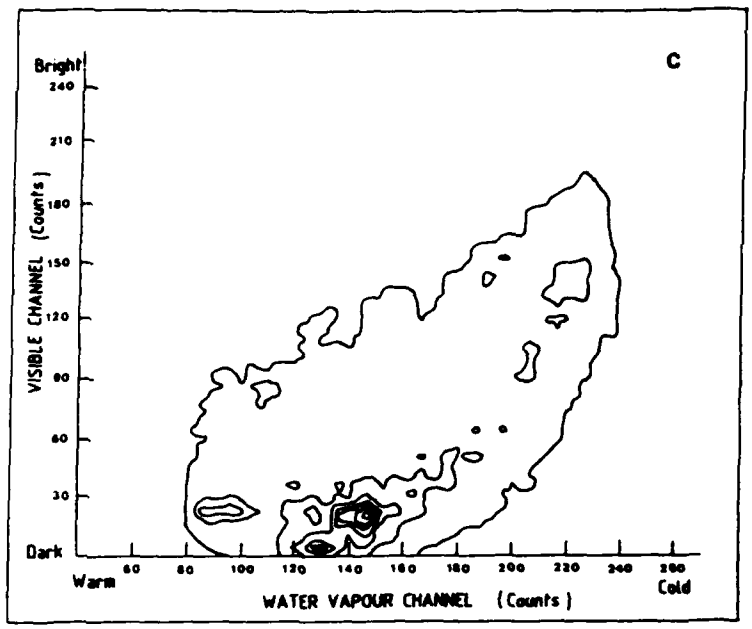

Figure 17 continued.

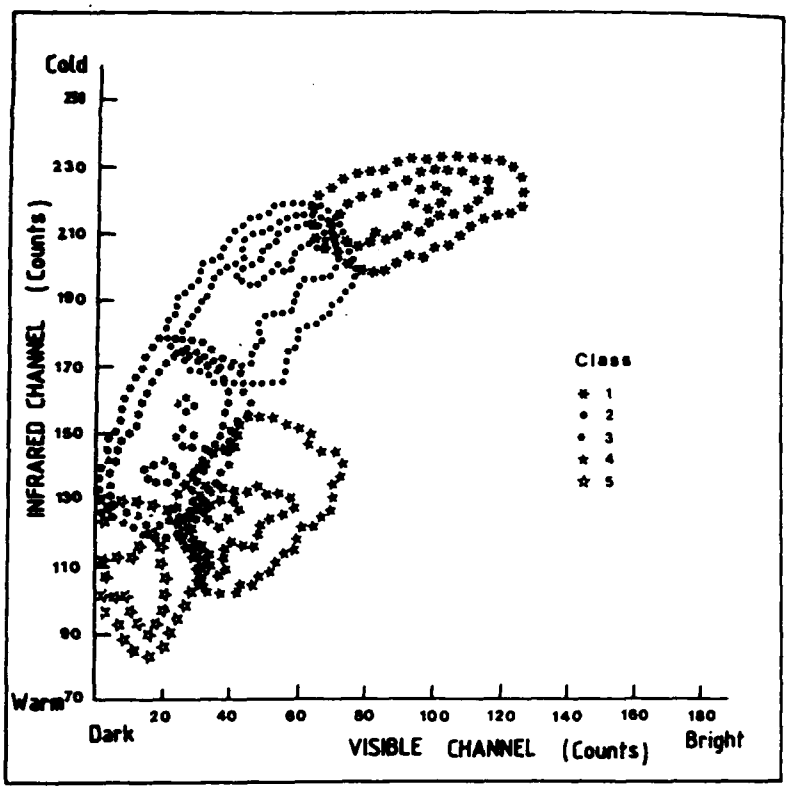

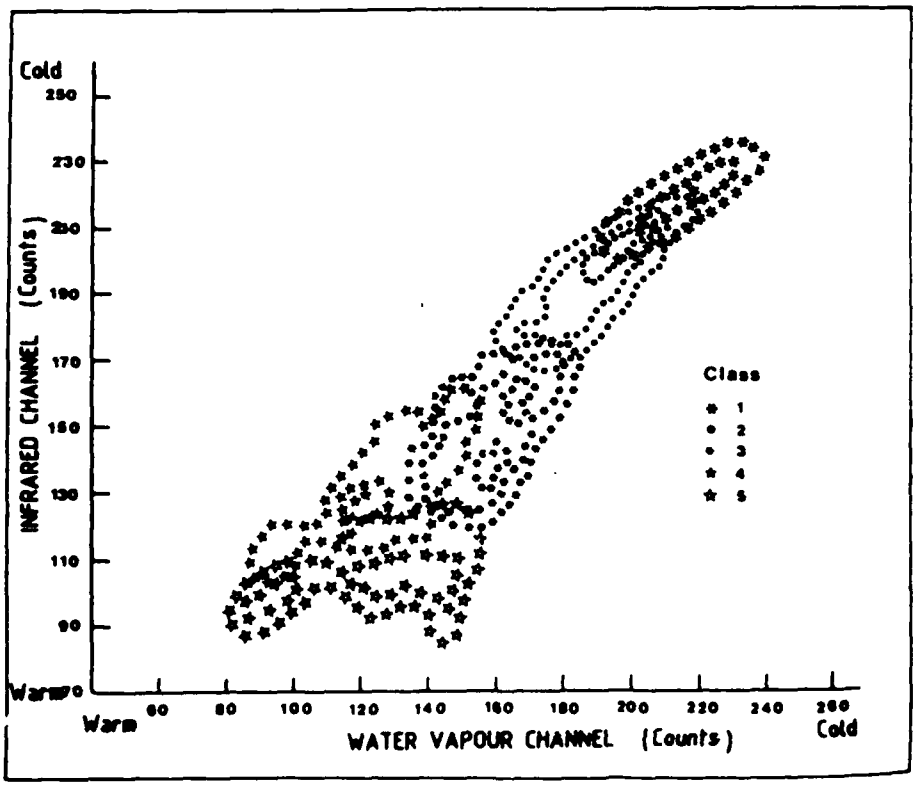

Figure 18 Classes obtained by the dynamic cluster algorithm for the same analysis region as in Figure 17, represented on two-dimensional histograms IR-VIS and IR-WV (after Desbois et al., 1982).

Table 4. Classes obtained for the same analysis region as for Figures 17 and 18. Percentage coverage of each class along with the centre of gravity and variance of each class are given. The units are numerical counts of the METEOSAT radiometers (after Desbois et al., 1982).

Classes	Percent coverage	VIS average (S.D.)	IR average (S.D.)	WV average (S.D.)
Large convective clouds	18	100 (15)	219 (10)	218 (14)
Edges of conv. clouds	18	56 (13)	195 (13)	191 (15)
Anvil cirrus	17	28 (9)	151 (14)	162 (13)
Low level clouds	7	54 (16)	134 (13)	129 (16)
Land and ocean	38	16 (8)	111 (9)	132 (19)

surface radiances from time series of images. Each image is extracted at the same time each day in order to avoid the requirements for corrections for variations in solar zenith angle. Also the use of raw METEOSAT radiometric counts for analysis avoids the use of calibration factors and angular and atmospheric corrections, all of which vary in accuracy. These stipulations amount to the requirement that observation conditions remain approximately constant throughout the period of image gathering. Sèze and Desbois (1986) discuss compositing techniques which are made rather complicated by the lack of correlation between minimum reflectance and maximum brightness temperature from pixel to pixel, a feature that often arises in the presence of very thin cirrus cloud. It is worth noting that information about daily cloud distributions and temperature maxima can also be ascertained from the infrared/visible histograms when certain cloud types are fairly clearly defined, such as cirrus, low level and multilayered clouds.

The use of spatial variances is designed to discriminate spectrally similar regions as well as provide information on partially cloud covered pixels (Coakley and Bretherton, 1982) (i.e. those regions where classes tend to overlap in two-dimensional histograms). Clouds (surfaces) of variable optical depth but uniform emissivity will have a high visible variance but low infrared variance such as low cumuliform clouds. The reverse applies to clouds of uniform optical depth and variable emissivity such as semi-transparent cirrus. The use of visible/infrared variance histograms is complementary to the radiance histograms which suggests that a four (five) parameter classification $IR/IR_{var}/VIS/VIS_{var}$ ($IR/IR_{var}/VIS/VIS_{var}/WV$) may help to separate further those cloud classes already broadly defined in the

original classification. Such a modified dynamic cluster analysis using four parameters is described in Seze and Desbois (1986). In this version the use of local variances improves discrimination of cirrus and improves the separation of totally cloudy classes from partially covered pixels.

The problem of treating partially cloudy pixels is well established. A novel approach to solving this problem has been proposed by Arking and Childs (1985). Their method is designed to treat pixels lying outside defined clusters and determine their cloud cover fraction whilst requiring that their other cloud parameters, optical depth (δ) and cloud top temperature (T_c), remain as consistent as possible with those of their nearest cluster.

The algorithm requires information from three AVHRR channels (1, 0.58 to 0.68 μm; 3, 3.55 to 3.93 μm and 4, 10.5 to 11.5 μm) and in the process retrieves four parameters, f, δ, T_c and a microphysical model index m describing the distribution of size, shape and refractive index of the cloud particles present in each pixel. Six possible values of m have been computed (Table 5). The basic radiative model assumes only one cloud type per pixel and uniform horizontal and vertical temperature and optical properties within each pixel. The retrieval (δ, T_c and m are determined once f is known) uses equations relating the three channel radiances measured for each pixel to the scene parameters within that pixel. A second radiative transfer model is thus built into the algorithm which is essentially a four-stage process, beginning with the determination of the clusters from histograms and subsequently the surface parameters for each channel. The microphysical model index appropriate to each pixel is found by

Table 5. Microphysical models (MPMs) and their optical parameters (after Arking and Childs, 1985).

MPM index	Mode radius (μm)	Particle phase	TIROS-N channel (μm)	Extinction coefficient (cm^2/particle)	Particle albedo	Asymmetry factor
1	4	liquid	0.73	1.66E-6	1.000	0.845
			3.7	2.01E-6	0.937	0.753
			11	0.88E-6	0.383	0.856
2	4	ice	0.73	1.68E-6	1.000	0.863
			3.7	1.98E-6	0.864	0.751
			11	1.16E-6	0.305	0.843
3	8	liquid	0.73	6.55E-6	1.000	0.863
			3.7	7.18E-6	0.878	0.820
			11	5.93E-6	0.494	0.936
4	8	ice	0.73	6.55E-6	1.000	0.871
			3.7	7.71E-6	0.799	0.837
			11	5.97E-6	0.411	0.927
5	16	liquid	0.73	2.57E-5	1.000	0.873
			3.7	2.73E-5	0.801	0.873
			11	2.83E-5	0.514	0.966
			0.73	1.02E-3	1.000	0.887
			3.7	1.06E-3	0.606	0.936
			11	1.05E-3	0.503	0.967

comparing the observed channel 3 radiance to that calculated for each index using model-derived values of δ and T_c (Figure 19).

Values of optical depth and cloud top temperature can be determined for all 'cluster-pixels' by application of the radiative transfer equations that effectively map visible reflectance and infrared brightness temperature into δ and T_c assuming f and m are known (f=1 for defined clusters). Recovery of whole image cloud statistics cannot be achieved however, until the values of f for partially cloudy pixels (i.e. those lying outside the clusters) have been determined. Maximal clustering is now invoked as follows. Figure 20 illustrates curves constructed from radiative transfer models describing the variation of δ and T_c with cloud cover fraction for a given visible reflectance, infrared brightness temperature and microphysical model index. The position of each pixel is allowed to vary along its respective curve until it lies closest to one of the clusters, in this way maximising the pixel concentration around the clusters. The value of f that corresponds to the new position of the pixel along its curve is set as the retrieved value of f, permitting δ and T_c to be determined (Figure 21).

The algorithm was tested on one of the ISCCP pilot study test regions, large enough to ensure stable statistics and a satisfactory level of consistency reached in a comparison with manually interpreted images. Use of the improved clustering method described would be a logical improvement and a direct comparison to results from the other clustering methods could serve to widen knowledge of this technique.

2.3 Spatial Coherence Algorithms

The major impetus for the study of local spatial variances (and their subsequent inclusion into dynamic cluster algorithms) was

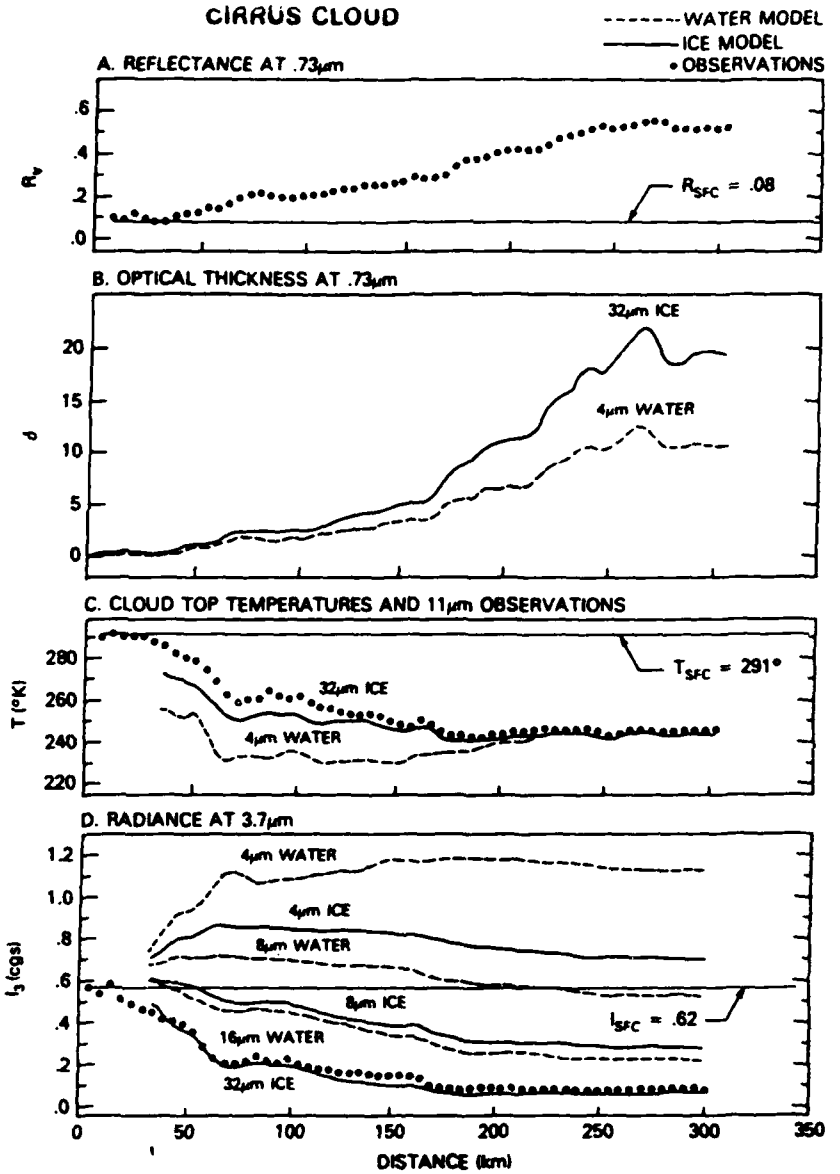

Figure 19

Observed and derived parameters along a NOAA-7 scan line. A) visible reflectance. B) calculated optical thickness that matches the measured reflectance for two microphysical models. C) calculated cloud top temperatures that correspond to the observed 11-micrometers brightness temperatures. D) calculated radiance at 3.7 micrometers based on derived values of δ and T_c for the 6 microphysical models compared with observations (after Arking and Childs, 1985).

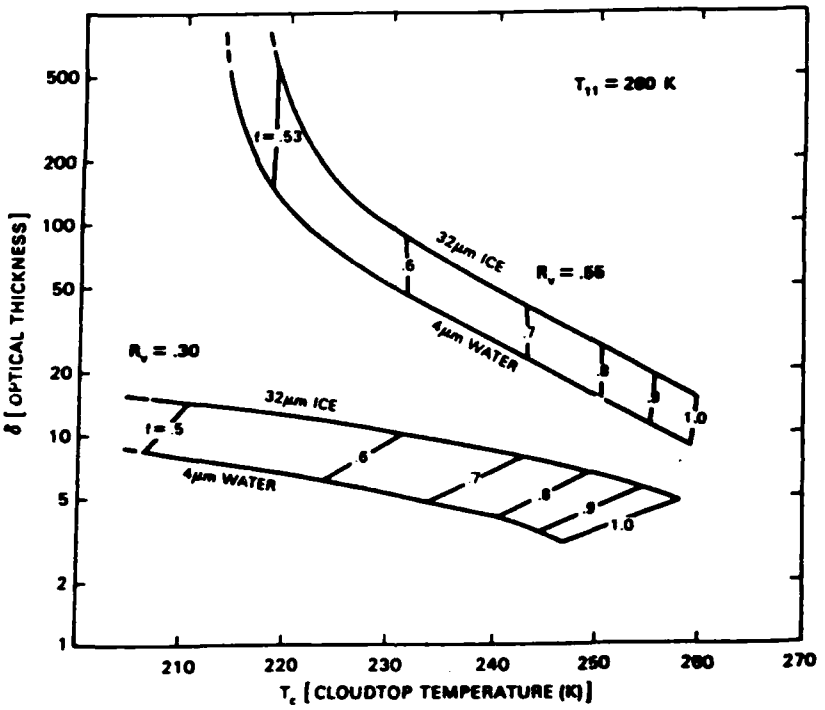

Figure 20 Possible values of the cloud parameters δ and T_c associated with a given 11 micrometers brightness temperature (T_{11}=260K) and two visible reflectances (R_V=0.30, 0.55) (after Arking and Childs, 1985).

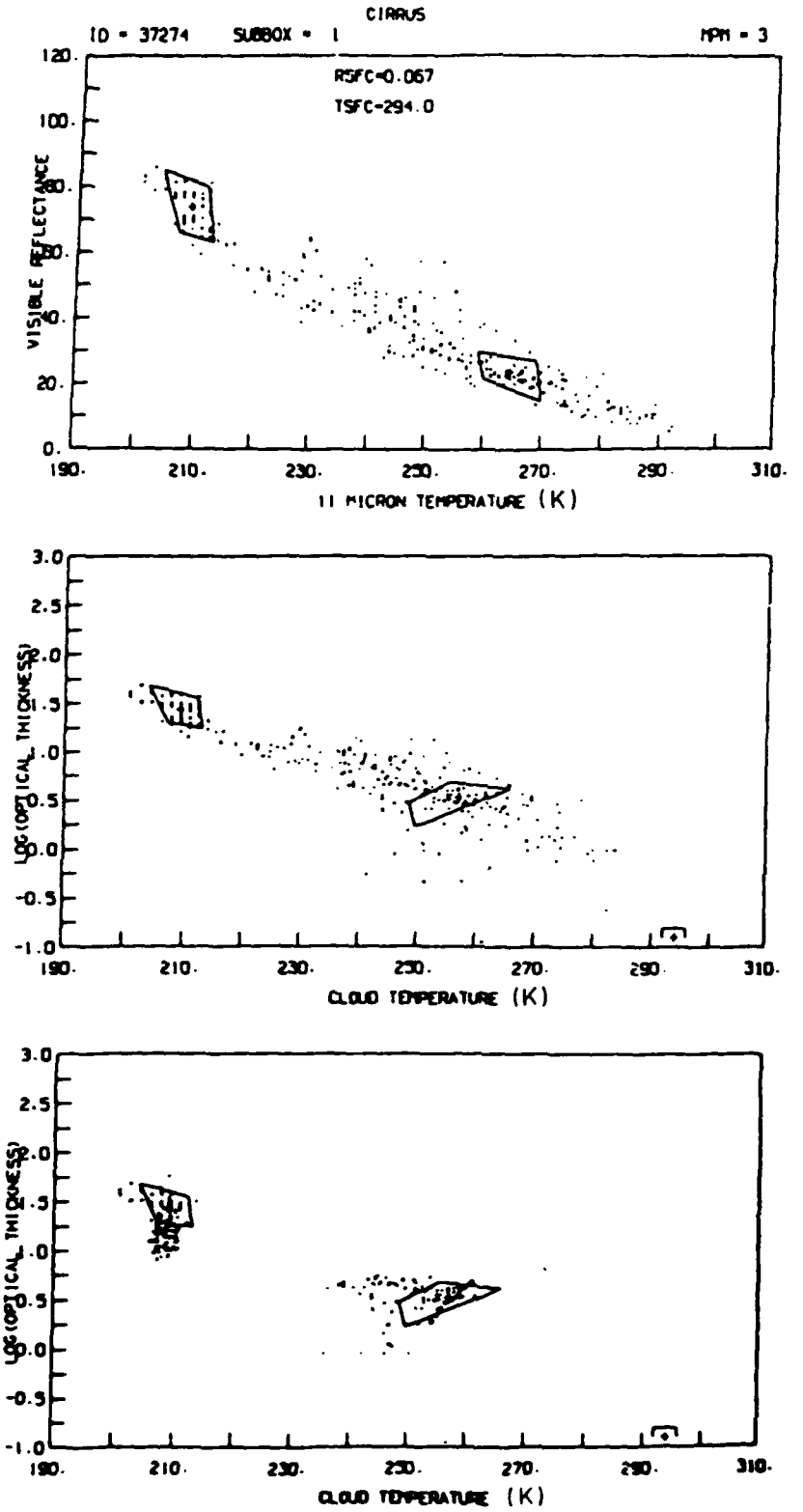

Figure 21 The selection of clusters in the visible (AVHRR channel 1) / infrared (AVHRR channel 4) two-dimensional histogram (top), transformation to the δ-T_c histogram, assuming completely cloud-covered pixels (middle) and the result of applying the 'maximal clustering' technique (bottom) (after Arking and Childs, 1985).

provided by Coakley and Bretherton (1982) who discovered that local variances, as applied to simple layered cloud systems could retrieve the radiances corresponding to the cloud free and cloud-covered fields of view, as well as those emanating from partially filled fields of view. The fundamental assumptions underlying their spatial coherence procedure are that a) the clouds are situated in distinct layers with each layer possessing a temperature appropriate to its altitude, and b) all the clouds in a layer emit radiation that is characteristic of the layer, the layers being optically thick at the observed wavelength with zero transmissivities. This being the case, when several cloud layers occur, each layer having at least several pixels width of non-overlapped cloud, the method permits the estimation of the radiances from the completely cloudy regions of each layer. By allowing detection only in the infrared channel the retrieval can be used to produce diurnal analyses.

To illustrate the simplest case the local standard deviation of 11 micrometer brightness temperatures is plotted in Figure 22 as a function of local mean radiating temperature for 8 x 8 pixel arrays (about 32km x 32km) of AVHRR global area coverage data for an oceanic region underlying a simple, homogeneous cloud layer. The result is an arch-like structure, typical of such plots, comprising two distinct clusters of low standard deviation points separated by a dispersion of higher standard deviation points. The 'warm' cluster centered on 293k $\pm$1k is attributed to homogeneous clear sky fields of view (ocean surface) whilst the colder cluster centered around 283.5k $\pm$1.5k corresponds to radiances emitted from completely cloudy pixels and the height of the cloud layer can be found from the difference in radiating

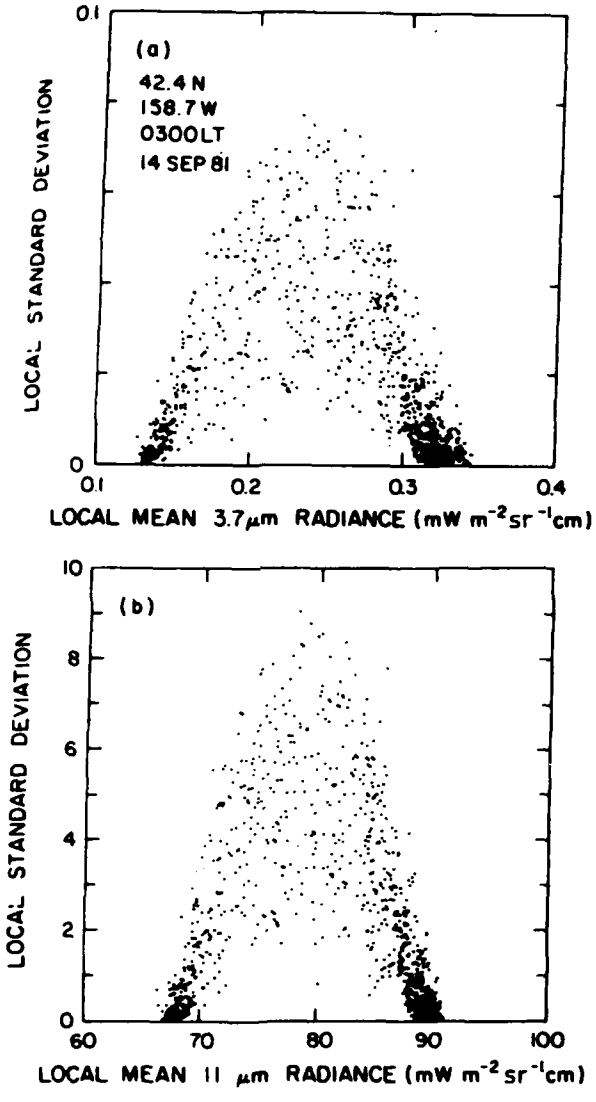

Figure 22 Local means and local standard deviations for the 3.7 micrometers and 11 micrometers channels for a simple one-layered cloud system over the Pacific Ocean (after Molnar and Coakley, 1985).

temperature. The points residing in the body of the arch are attributed to partially filled pixels (with f decreasing as we increase the radiating temperature from 283.5k) as these pixels should not be expected to possess the same degree of local coherence as those from clear or cloudy regions. Hence since the presence of a layer can only be detected when adjacent fields of view are completely filled this retrieval method is successful only when the cloud cover is uniform over areas considerably larger than the resolution of the data. If this crieterion is not met, the resulting plot could not be used to determine the cloud's radiating temperature. Those cloud types exhibiting considerable spatial structure such as developing cumulus congestus and cirrus are therefore less likely to be detected as a layer.

Estimation of fractional cloud cover (A_c) for regions comprising single layer systems is given by

$$A_c = (I - I_s)/(I_c - I_s) \qquad (1)$$

where I is the mean radiance, defined by

$$I = (1 - A_c)\, I_s + A_c I_c \qquad (2)$$

where I_s, the clear sky radiance, and I_c, the cloudy radiance are both derived from the position of the "feet" of the arches. The uncertainty in A_c can be estimated once the uncertainties in I_s and I_c are known since they are proportional to the breadth of the arch feet. Any uncertainty in I is the result of instrument noise and is of negligible magnitude. Note that the method, applied to clear sky conditions over oceanic regions, will provide a useful guide to sea surface temperature (by applying the inverse Planck function to the clear sky radiance value), although with greater uncertainty compared to values obtained from sounding.

Because persistent single-layered cloud regimes (e.g. marine stratocumulus near coastal South-West Africa) are fairly scarce and the majority of cloud systems around the globe comprise two or more distinct layers, the ideas of spatial coherence were extended to multilayered systems (Coakley, 1983). When two layers appear in a scene the points in the bodies of the resulting arches denote contributions of cloud cover from both layers as in Figure 23. Specifically in Figure 23(a) (Figure 23(b)) the regions of locally uniform emission are observed at approximately 88, 68 and 37 mW m^{-2} sr^{-1} cm (0.30, 0.14 and 0.03 mW m^{-2} sr^{-1} cm). The arch foot at 88 (0.30) mW m^{-2} sr^{-1} cm is interpreted as being due to radiation from the cloud free oceanic background whereas the two remaining feet are interpreted as lower and upper level cloud layers respectively. All the pixels not yet accounted for are designated as partially covered with an as yet unknown combination of clouds from the two layers. If the fractional contribution of each layer is known then the total fractional cover can be found. Figure 24 shows a spatial coherence plot for the sub-scene frame C [42 ^{o} - 47^{o}] of the NOAA AVHRR data from Figure 1, depicting some uncertainty in the definition of the arches. Three arch feet are discernible, that centered on 360 counts referring to the land surface background whilst the major cloud decks present give rise to the feet centered at 570 and 760 counts. The breadth of the arch feet and the large number of pixels within the (ill-defined) arches suggest that in this case a poor result for A_c would be obtained. This illustrates some of the problems of performing spatial coherence retrievals against (i) a non-uniform land surface and (ii) a rather complex cloud pattern. Coakley (1983) used simultaneous

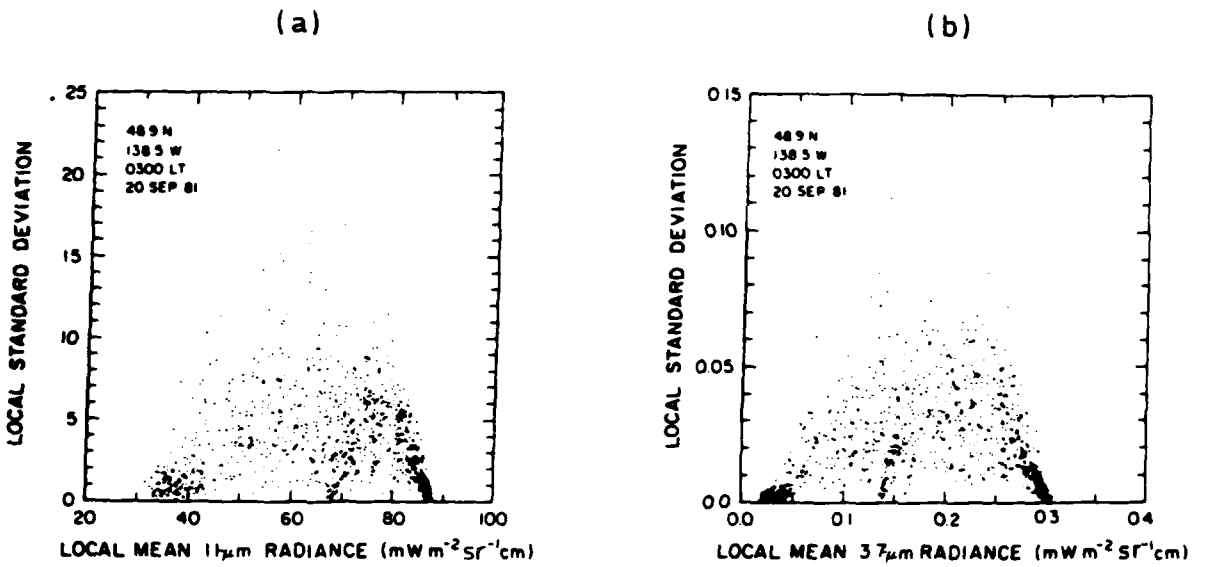

Figure 23(a) Local means and local standard deviations of 11 micrometers radiances for 2 x 2 pixel arrays (4 km x 4 km) from the NOAA-7 AVHRR. The data are for a nighttime pass over a (250 km x 250 km) region of the Pacific Ocean centered at 48.9°N, 138.5°W (after Coakley, 1983).

Figure 23(b) Local means and local standard deviations of 3.7 micrometers radiances for the same pixels as in Figure 23(a) (after Coakley, 1983).

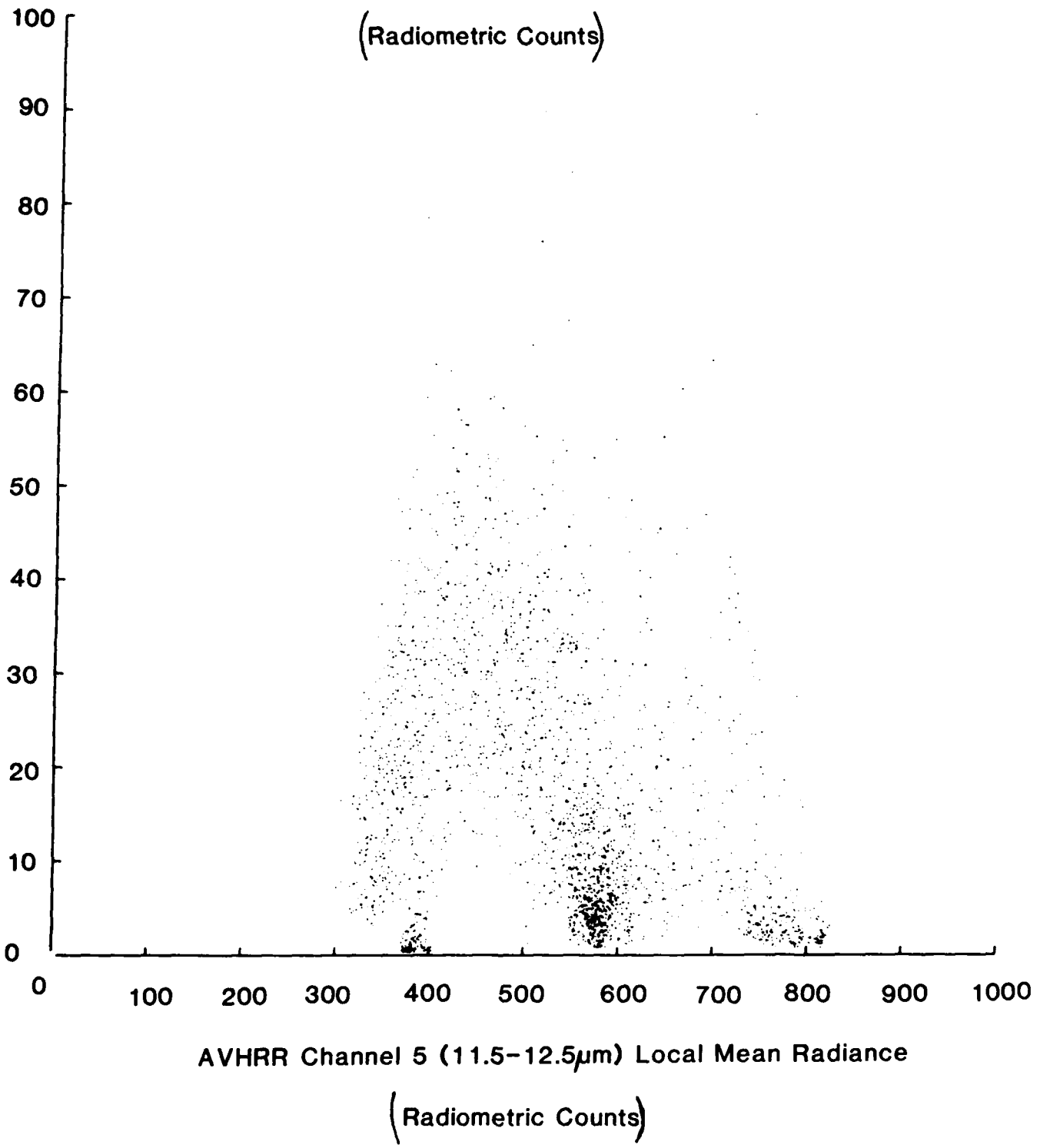

Figure 24 Spatial coherence plot of local mean infrared (AVHRR channel 5, 11.5 - 12.5 μm) versus local infrared standard deviation for 3x3 pixel arrays from the sub-scene, frame C (42° - 47°) of the data shown in Figure 1.

observations in the 3.7 micrometers window (channel 3 AVHRR) and the 11 micrometers window (channel 4 AVHRR), (these channels being linearly independent from each other) to obtain the non-overlapping fractional cover attributed to each of the two layers by solving pairs of simultaneous linear equations such as those below. For observations in channels I and J, and for two cloud layers 1 (the lowest layer) and 2 (the upper layer)

$$I^i = (1 - A_{c1} - A_{c2})\, I_{si} + A_{c1}\, \epsilon_1^i\, I_{c1}^i + A_{c2}\, \epsilon_2^i\, I_{c2}^i \qquad (3)$$

$$I^j = (1 - A_{c1} - A_{c2})\, I_{sj} + A_{c1}\, \epsilon_1^j\, I_{c1}^j + A_{c2}\, \epsilon_2^j\, I_{c2}^j \qquad (4)$$

where I^i is the radiance received in channel i; A_{c1} is the fractional area of a pixel covered by clouds from layer 1 that are not overlapped by layer 2 clouds; A_{c2} is the fractional pixel area covered by only layer 2 clouds; Is^i is the clear-sky radiance in channel i and $\epsilon_1^i I_{c1}^i$ represents the radiance observed for pixels cloud-covered by layer 1 with no overlapping layer 2 clouds, ϵ_1^i being the emissivity of the optically thick layer 1 cloud in channel i. Similarly $\epsilon_2^i I_{c2}^i$ is the radiance from pixels completely covered by layer 2 clouds. Whilst $\epsilon^{i,j}$ and $Ic^{i,j}$ values are not known separately the values of their product terms in Equations (3) and (4) are derived from the feet of the arches, as in Figures 23 and 24. Solution of Equations (3) and (4) for A_{c1} and A_{c2} is straightforward in an ideal situation.

However, with the likely uncertainties in I_s, I_{c1} and I_{c2} noted Coakley (1983) has determined a stability condition for the equations which indicates when they cease to be linearly independent. Satisfaction of this condition entails that whatever applies to two layers can apply equally to three. However, the number of linearly

independent and widely spaced infrared channels is a limiting factor, indeed the use of the 3.7 micrometers and 11 micrometers channels together permits only nighttime observations due to daytime reflection of solar radiation by low-level water clouds in channel 3. The window at 2.3 micrometers is as yet unexplored but may be studied in future from Landsat measurements. Of high importance is the need to test the validity of the underlying assumptions prior to testing. Coakley's major conclusion was that cloud systems forming arches from a spatial coherence analysis almost always satisfy both layer and optical thickness assumptions. Data presented in Coakley (1983) were extracted from tropical and mid-latitude Pacific regions and excluded continental areas where clear sky properties are more variable. The results showed promise but would benefit from comparison with in-situ data.

The suitability of the spatial coherence technique to maritime environments was further underlined by Coakley and Baldwin (1984) who adopted a strategy of analysing smaller (60 km x 60 km) subregions in preference to 250 km x 250 km areas, compositing the subregion statistics to provide larger scale results. Apart from reducing the data input volume by more than an order of magnitude the cloud patterns encountered in the subregions were almost always one or two-layered and were thus conducive to analysis by spatial coherence. Complex systems such as frontal clouds and large convective systems (those for which spatial coherence cannot provide realistic retrievals) were treated with a default estimate [see Coakley and Baldwin (1984) for full description]. This, by definition, incorporated greater uncertainty than the spatial coherence retrievals. For the area studied, those oceanic regions which were frequented by the 'awkward' systems suffered from larger uncertainties

in mean cloudiness as compared with those areas dominated by layered cloud formations.

Validation

This approach suggests itself as a possible ISCCP maritime retrieval algorithm (at least in areas where the climatological cloud patterns indicate its potential applicability), but the results for landmasses (although yet to be analysed) are unlikely to be so promising, particularly in mid-latitudes. An alternative channel to 3.7 micrometers needs to be found for daytime retrievals [one recently proposed alternative is the snow / cloud discrimination channel centred at 1.6 micrometers] and corrections for viewing geometry have not been considered.

The most recent development in this area is the work of Molnar and Coakley (1985) who assembled data sets for single and two-layered cloud systems for which the spatial coherence technique provided reliable results and which were statistically independent of one another. Using these examples they were able to demonstrate similarities in cloud cover patterns for large and small sub-scenes. This discovery may be of interest to climate modellers who wish to represent the effect of sub-grid scale clouds. The analysis was subsequently used to design a statistically-based algorithm which, using simple mathematical models is intended to fit the correct value of mean cloudiness over all the partially cloudy pixels. Initial results were compared to those derived from spatial coherence with good consistency achieved. Total cloud amount was slightly underestimated in double-layered cases and similar errors were predicted for cloud systems of greater complexity. Because the method had no fundamental

dependence on spatial coherence assumptions Molnar and Coakley (1985) emphasised its potential value in "difficult" areas. Results of further tests are now required. Overall the status of spatial coherence methods for cloud retrieval is one of limited success so far but clearly worthy for future development.

2.4 Radiative Transfer - type Algorithms

This, the third major class of retrieval algorithms employs an entirely different methodology from the retrieval techniques described so far. Here the cloud parameters are determined from the fitting of atmospheric radiative transfer models to the observed radiances. The models differ in their complexity according to the number of wavelength channels used and most employ some auxiliary data to improve the accuracy of retrieval (Reynolds and Vonder Haar, 1977; Platt, 1983; Rossow et al., 1985).

Methods of calibrating absolutely infrared radiances from several spectral channels against appropriate models in order to infer cloud properties has been put forward by Chahine (1982) as a co-product of vertical temperature profile and humidity distribution retrievals. In this method the technique is to obtain first the cloud free radiances by comparing the radiances measured in adjacent areas, assuming variations in the cloud properties within the comparison region. The model employed describes both cloud radiative properties and cloud vertical distribution and is used in the comparison of the observed radiances to the estimated cloud free values to extract the cloud properties.

As the number of spectral channels used increases so increasingly complex cloud models can be employed and it should be possible, with sufficient channels, to model effectively multilayered cloud systems

and increase the accuracy of retrieval in such cases. At present, however, the procedure utilises only three channels and can derive f and cloud top height for simple (i.e. single cloud layer) models. Tests so far indicate good agreement in the case of optically thick cloud with large deviations encountered for thin high clouds. This difference in results for low and high clouds has hindered the progress of this type of radiative transfer algorithm. Future improvements rest on the inclusion of extra spectral bands and model refinements.

The bispectral technique developed by Reynolds and Vonder Haar (1977) examines each pixel's net radiation balance, relating the radiances received in both visible and infrared channels to the sum of the contributions from clear and cloudy regions within the field of view. Input parameters to the model include surface temperature, visible albedos, infrared emissivities and visible bidirectional reflectances which are used to calculate the fractional radiance contributions for an idealised single layer cloud. The second step uses the radiances to calculate the cloud fraction and cloud top temperature for each pixel. Vertical temperature profile retrievals can be used to equate T_c with cloud top height. This method allows correction for viewing geometry and varying surface properties, important features which the previously described algorithms do not incorporate. The test site used had the advantage of a high density of surface observers and in a comparison study very good agreement was reached with them with the exception of cirrus where local variations in optical depth were misinterpreted as variations in cloudtop height and f. The model had associated a constant emissivity for cirrus clouds but subsequently a new algorithm was devised for cirrus clouds

in which an attempt was made to calculate emissivity as a direct function of visible albedo. This greatly improved cirrus retrievals. The other major 'problem' cloud type, that of boundary layer cumulus was well retrieved by this technique.

A 'dynamic' radiation budget approach, as opposed to the 'static' radiation balance described above, has been proposed by Smith and Vonder Haar (1983). The improvement here concerns the determination of the cloud and surface radiative properties from the satellite data itself instead of from 'static' model comparisons. Much of the methodology appears in previously discussed algorithms. Firstly, the surface radiative properties are deduced from time-period composites (15 days) of minimum reflectance and maximum brightness temperature for each pixel location. The composites must then be spatially averaged if mean surface radiative properties are to be determined for small sub-regions. Application of an appropriate clustering technique (Everitt, 1980) to bispectral radiance histograms generates clusters representing the various cloud types present, each cluster center defining a particular visible albedo and cloud top temperature. Climatological temperature profiles are used to equate each T_c with a cloud top height.

A similar radiative model to that used in Reynolds and Vonder Haar (1977) is used to estimate cloud cover fraction, f. It is assumed that the measured mean radiances are again a function of the combined clear and cloudy radiance terms. The problems of variable infrared emissivities resulting from varying optical depth are overcome as previously by the inclusion of an emissivity-reflectance function whilst corrective terms for atmospheric attenuation in the infrared (mainly due to water vapour absorption) and viewing geometry

are also included. In order to perform on a diurnal basis the algorithm employs an infrared threshold during nighttime, defined so as to reduce the mean square difference in retrieved daytime cloud amount between itself and the dynamic bispectral method, thus assuming that the most suitable threshold can be used irrespective of the time of day. The method achieved a satisfactory level of success in preliminary tests with the exception of thin cirrus. Its merit relative to its predecessor is as yet unclear and a direct comparison would be a useful exercise.

Occasionally radiative transfer methods include threshold or statistical elements in their framework (Rossow et al., 1985). A surface/atmosphere/single cloud layer model is utilised here and model radiances calculated as a function of the surface properties, cloud properties, vertical profiles of temperature, humidity and ozone abundance, along with viewing geometry.

The main points of the model are described as follows. The atmosphere is composed of a Rayleigh scattering gas residing underneath and above a single layer of cloud. Its vertical temperature profile is determined from climatological daily average values. The cloud layer is assumed to be plane-parallel comprising water spheres whose effective mean radius is 10 micrometers. Visible reflectivity, transmissivity and infrared emittance are all characteristic of such a surface. Incoming solar radiation is partially attenuated by atmospheric ozone whose distribution is provided from a seasonal zonal mean climatology (see Hilsenrath and Schlesinger, 1981). The land surface is depicted as an isotropic reflector with a reflectivity that varies with position whilst all the

surface is assigned a unit emissivity in the infrared. The ocean surface likewise has unit infrared emissivity whilst its reflectivity is governed by Fresnel reflection coefficients (see Cox and Munk, 1956). Finally weighted reflectivities are introduced to any region experiencing snow cover (this applied to one of the test regions when the model was employed in the ISCCP pilot study).

After comparing the model radiances with the observed values, simultaneous infrared and visible thresholds (infrared only at night) are applied to the deduced cloud properties, the criterion being that both must be exceeded in order to count a pixel as cloudy. Since the thresholds are applied to cloud properties which result directly from observed versus model radiance comparisons, they do not resemble fixed radiance increments like the previous thresholds. The results from the testing of this algorithm in the ISCCP pilot study were dominated by its repeated failure to detect low lying clouds whilst remaining clouds were retrieved satisfactorily.

A third bispectral technique involving the comparison of bispectral curves of visible albedo versus infrared brightness temperature from "real" clouds to model curves for extraction of cloud fraction and optical depth is given in Platt (1983). Model curves have been constructed for idealised single and multilayered clouds and compared to bispectral histograms determined from observed satellite data.

Each idealised cloud layer is characterised by an optical depth that, although constant within an individual pixel, may vary between adjacent pixels. The value of f is permitted to vary from one pixel to the next but the cloud top within a layer is set at a constant height. The actual cloud is defined as a homogeneous isothermal

region whilst scattering effects are limited to incoming solar radiation which the layer scatters isotropically. The underlying surface has unit infrared emissivity, a visible albedo resembling that of an ocean surface and is assumed to be isotropic as well as homogeneous. Equations for the visible and infrared radiances from 'model' clouds that might be received by a satellite, are then formulated. These include albedo, emissivity, pixel cloud fraction and optical depth terms and provide the theoretical basis upon which the curves are constructed (Figure 25(a)). The parameters used in the single layer calculations are shown in Table 6.

The curves depict albedo/brightness temperature relationships for clouds forming (i) a continuous layer with varying optical depth and (ii) a broken layer with uniform optical depth. In this way changes in cloud amount and optical depth can be related to changes in albedo and temperature. Curves 1 and 2 could be said to depict crudely, in the high cloud case, cirrus and cirrocumulus clouds respectively whilst in the low cloud case they might characterise stratus and stratocumulus respectively. The sensitivity of the model to cloud detection will depend on the albedo and temperature resolution of the observations and on the data array having a smaller dispersion than the distance between curves 1 and 2. There is, of course, the additional possibility of further model refinement. The theory discussed by Platt (1983) also permits the calculation of cloud fraction and emissivity for each pixel within a single cloud layer.

The method has been extended to account for variations of albedo with solar zenith angle, variations of brightness temperature with satellite viewing angle and cases where multiple cloud layers overlap

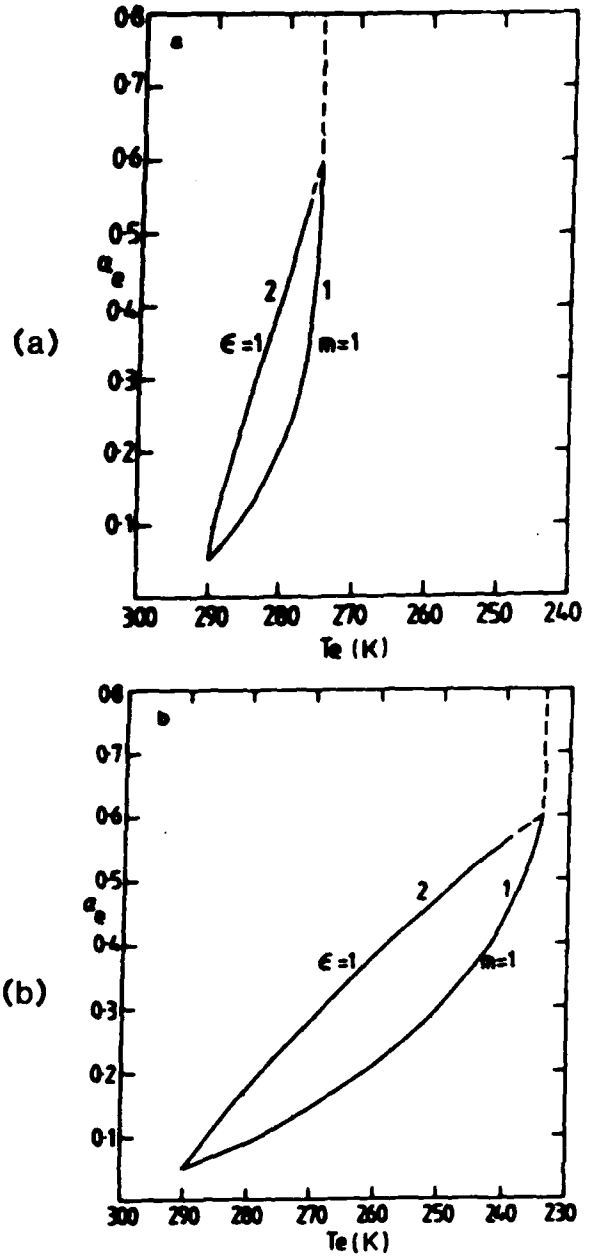

Figure 25(a) Bispectral curves of albedo, α_e, versus brightness temperature, T_e for a low cloud layer. Line 1 represents an unbroken layer with variable optical depth whilst line 2 is for broken layer of constant optical depth cloud (after Platt, 1983).

Figure 25(b) As for Figure 25(a) but for a high cloud layer (after Platt, 1983).

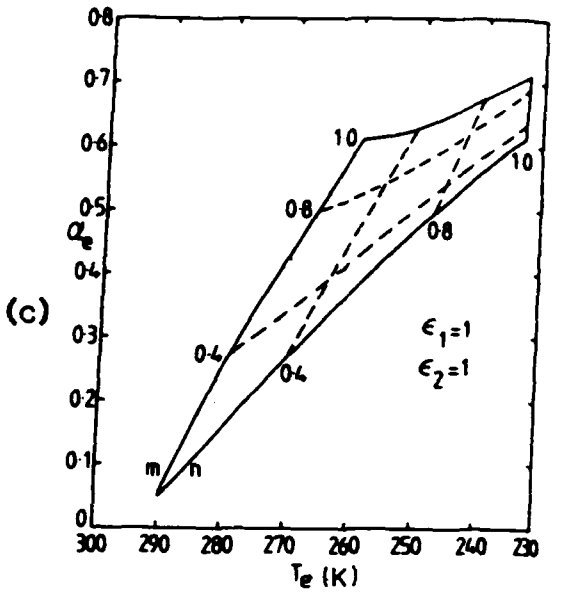

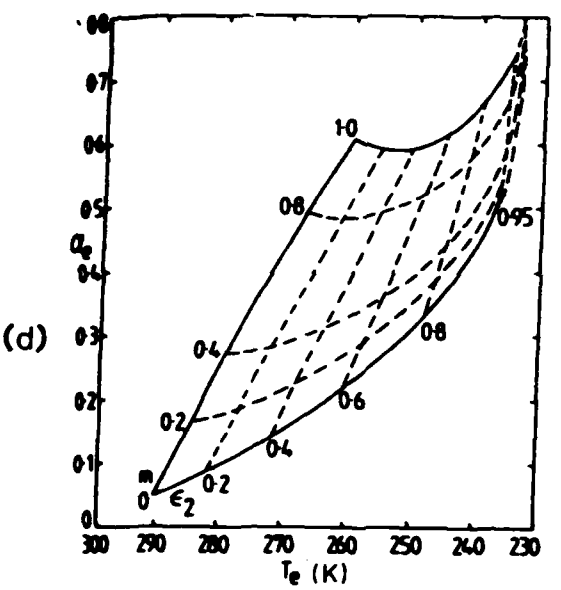

Figure 25(c) Bispectral curves of albedo, α_e, versus brightness temperature, T_e, for two overlapping cloud layers. The layers are broken but cloudy regions have uniform optical depth (after Platt, 1983).

Figure 25(d) Bispectral curves of albedo, α_e, versus brightness temperature, T_e, for two overlapping cloud layers in which the top layer is unbroken, comprising cloud of variable optical depth whilst the bottom layer is broken with cloud of uniform optical depth (after Platt, 1983).

Table 6. Parameters employed in single cloud layer calculations. T_c and T_g are the cloud and surface temperatures respectively α_g is the surface albedo, θ represents the incidence angle of solar radiation at the cloud whilst ξ denotes the nadir angle of the cloud at the satellite. $\alpha(\delta_c,\theta)$ is the cloud albedo as a function of its visible optical depth and solar radiation incidence angle whilst g is the ratio of visible optical depth divided by the infrared absorption optical depth (after Platt, 1963).

	Boundary layer cloud	High cloud
T_c(K)	275	233
T_g(k)	290	290
α_g	0.05	0.05
Phase	Water	Ice
θ (deg)	30	30
ξ (deg)	0	0
$\alpha(\delta_c,\theta)$	0.6	0.6
g	2.5	2.0

each other. In the latter case the shape of the curves is determined by four independent variables namely, the cloud fraction and emissivity of the two overlapping layers. Figures 25(b) and 25(c) illustrate curves depicting typical atmospheric cloud systems. The basic equations have been simplified here for cases of cirrocumulus overlying altocumulus (Figure 25(b)) and cirrostratus overlying cumulus (or altocumulus) (Figure 25(c)). Again variations in layer cloud fraction and cloud emissivity are reflected in albedo and brightness temperature changes. In addition Platt (1983) illustrates the possible effects due to infrared scattering when the cloud layers become deeper and the model assumption of an isothermal cloud becomes invalid.

The model curves have been tested against multiple cloud layer systems over ocean and land surfaces. Albedo/brightness temperature histograms are constructed from satellite measurements and model curves fitted to assess the level of agreement. Figure 26 shows the result of fitting a model curve for semitransparent cloud to a bispectral histogram for data from a complex tropical convective system. The consistency is evident along much of the histogram's major axis auguring well for the model structure in this case.

The overall value of this radiative transfer algorithm is so far unknown. More comprehensive model tests are still necessary, particularly on convective and frontal clouds, as well as on low level stratus which require the inclusion of features such as anisotropic cloud reflection into the model. Platt (1983) reports that any future development leading to possible incorporation into the ISCCP algorithm will have to follow identification of a successful method for automating the removal of cloud parameters from the input bispectral

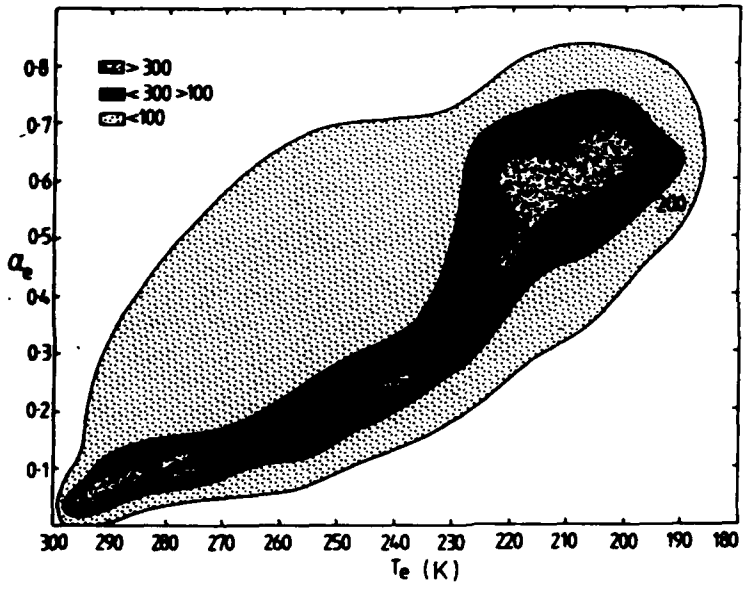

Figure 26 Two-dimensional bispectral histogram for a 500 km x 500 km area containing tropical clouds on 11 April 1980, latitude 2.5°N, longitude 137.5°E. The lines represent two predicted bispectral curves for a single layer of semitransparent cloud with cloud top temperatures of 200 and 210 K, respectively (after Platt, 1983).

data.

3 Feasibility of Using Surface Observations

Throughout the discussion of retrieval algorithms in Section 2 the need for improved development and subsequent testing has been emphasised because many of the methods are still in their infancy and have been tested only on limited regions on a limited time scale in the course of which the full range of conditions, heterogeneous surface properties, time-varying surface problems and all the major global cloud systems have not been encountered. The aim of those involved in the ISCCP pilot study in 1981 was to try to rectify this in part but the caveats still apply to developments that have taken place since (spatial coherence, maximal clustering, bispectral curves). Perhaps the most pertinent problem to climate modellers at present is the lack of a uniform global cloud climatology. The data set that will hopefully emerge from ISCCP will be wholly satellite based. The retrieval algorithm that was proposed, after the pilot study was not specifically any of those tested but combined the 'best' features of some of the individual methodologies. There will, however, still remain the problem of how to validate the data set. The most readily available method (and perhaps the only conceivable one) lies in comparison with surface synoptic reports but the paucity of such exercises (Reynolds and Vonder Haar, 1977) had until recently left something of a void in this area.

The problems of satellite retrieval are now fairly well established (Rossow et al., 1985) and the question arises can surface observations be added to or in some way calibrated to satellite retrievals so as to improve the quality of the latter. The problem is

addressed by Sèze et al. (1987) which describes details of a 20 day period in the summer of 1983 during which satellite to surface cloud amount comparisons were made over western Europe using data from surface stations in Britain and France and the corresponding METEOSAT imagery. The exercise formed a part of the ISCCP preliminary validation exercise and was colocated with one of the special study regions designated by ISCCP. Methods of the surface retrieval are given in Sèze et al. (1987) whilst the satellite algorithm was the four-parameter ($IR/IR_{var}/VIS/VIS_{var}$) clustering technique (Desbois and Sèze, 1984a).

Overall, the level of agreement in total cloud amount between satellite and surface observer was $\pm$ 1 okta (or $\pm$12%) for 64% of all cases. The study raises many interesting and pertinent points which are considered briefly here.

Beginning with total cloud amount, there was found to be greatest agreement in either clear sky situations or single-layered complete overcasts but low cloud amounts (important for considering surface radiative fluxes) were considerably underestimated by the satellite whenever middle or upper level cloud overlaid the low cloud deck. This is possibly a case in which surface reports could assist in correcting satellite measurements (layer obscuration). Correspondingly it was found that the surface observer underestimated high cloud amount (>6 km altitude) when it was obscured from view by lower decks. In this situation the success with which the algorithm was found to detect cirriform clouds well, becomes important. In this study serious discrepancies arose for such cases, which were directly related to the success with which the algorithm could detect cirrus cloud. Ideally the surface data could be compared with the results of

a wide range of alternative algorithms.

The use of METEOSAT radiances at middle latitudes raises problems of viewing geometry and the pixel resolution of 6 km x 6 km means that many pixels may be partially cloud covered. At the latitudes concerned METEOSAT will view the sides of clouds, particularly those of developing cumuliform clouds which were observed to occur and small gaps in layers will also be missed. However, perspective problems are not confined to the satellite alone. The surface observer also fails to detect gaps in the cloud cover at low elevation angles (Malberg, 1973) and tends to overestimate cloud amount near to the horizon (Merritt, 1966). The perspective effects can be shown to be of similar magnitude for both surface and satellite retrievals but should not be disregarded altogether.

The representativeness of the surface stations is another important area. In an ideal comparison a spatially homogeneous, dense observing network could be colocated with the satellite image pixels. Reality is far removed however, and considerations to the area representative of each surface station are given in Seze et al. (1986, 1987). It should also be conceded that a surface observer is an essentially subjective analysis instrument. Perhaps the use of all-sky cameras could provide a more objective retrieval (Ackerman and Cox, 1981).

The question of incorporating surface observations into the satellite retrieval remains a very difficult one. A method of combining the two data types realistically has yet to be proposed. One possibility concerns the work of Hahn et al. (1984) which consists of surface-derived cloud climatologies expressing the probability that

given the presence of one cloud type, another type is present. If the satellite-derived cloud type is assumed to be the referenced type the extra information provided by these climatologies could improve future retrievals.

Much work remains to be done on algorithm testing, improvement and validation. It now appears certain that any future global retrieval algorithm will be a heterogeneous composite of a range of satellite-based techniques. It is therefore reasonable to propose the inclusion of surface observations where they would improve the cloud characterisation.

4 Summary and Conclusions

This report describes the first phase of a three year study of cloud retrieval techniques. The aim this year has been to review existing techniques with particular attention being paid to satellite-based retrievals and to novel proposals made since the ISCCP intercomparison was initiated in 1981/82. The somewhat unsatisfactory conclusion that must be drawn is that while many new techniques offer useful, even uniquely successful, retrieval capabilities in certain well-defined situations they have not yet, and perhaps can never, be shown to be applicable to other areas, climates and configurations.

Two recommendations are made: (i) there should be a broader "validation" of many of the techniques reviewed here and (ii) an attempt should be made to incorporate surface-based observations in retrievals. It seems likely that in many situations surface-based observations offer the only satisfactory means of detecting (a) small-scale structure, especially fair weather cumulus and gaps in cloud decks, (b) thin cirrus and (c) low cloud amount and type in the presence of middle and high cloud layers. These preliminary

conclusions seem to justify the U.S. Air Force's use of "all available data" in their construction of global nephanalyses.

5 Presentations and Publications

As most of this year's work has been of an introductory nature consisting primarily of literature review no publications have ensued.

Two presentations have been made:

Postgraduate seminar series at Liverpool University on 19th June 1986 entitled

"Automated analyses of satellite radiance data".

Seminar at NATO School on Remote Sensing in Meteorology and Climatology in Dundee (Aug. / Sept. 1986) entitled

"A brief introduction to satellite cloud retrieval"

6 References

Ackerman, S.A., and S.K. Cox, 1981, Comparison of satellite and all-sky camera estimates of cloud cover during GATE, J. Appl. Meteor., 20, 581-587.

Arking, A., 1964, Latitudinal distribution of cloud cover from TIROS III photographs, Science, 143, 569-572.

Arking, A., and J.D. Childs, 1985, Retrieval of cloud cover parameters from multispectral satellite measurements, J. Climate Appl. Meteor., 24, 322-333.

Barnes, J.C., and D. Chang, 1968, Accurate cloud cover determination and its effects on albedo computations. Final Report 9G53-12. Allied Research Associates Inc., Concord, Mass.

Chahine, M.T., 1982, Remote sensing of cloud parameters, J. Atmos. Sci., 39, 159-170.

Clapp, P.F., 1964, Global cloud cover for seasons using TIROS nephanalyses, Mon. Weather Rev., 92, 495-507.

Coakley, J.A., and F.P. Bretherton, 1982, Cloud cover from high resolution scanner data: detecting and allowing for partially filled fields of view, J. Geophys. Res., 87, 4917-4932.

Coakley, J.A., 1983, Properties of multilayered cloud systems from satellite imagery, J. Geophys. Res., 88, 10808-10830.

Coakley, J.A., and D.G. Baldwin, 1984, Towards the objective analysis of clouds from satellite imagery data. J. Climate Appl. Meteor., 23, 1065-1099.

Cox, C., and W. Munk, 1956, Slopes of the sea surface deduced from photographs of the sun glitter, Bull. Scripps Inst. Oceanogr., 6, 401-488.

Desbois, M., G. Sèze and G. Szejwach, 1982, Automatic classification of clouds on METEOSAT imagery: application to high-level clouds, J. Appl. Meteor., 21, 401-412.

Desbois, M., and G. Sèze, 1984a, Use of space and time sampling to produce representative satellite cloud classifications, Ann. Geophys., 599-606.

Desbois, M., and G. Sèze, 1984b, Application of a clustering method for cloud cover analysis over tropical regions. Prepr. from Workshop on Cloud Cover and Radiative Fluxes in large-scale Numerical Models, ECMWF, Reading, November 1984.

Everitt, B., 1980, Cluster Analysis, (2nd Edition), Halsted Press, New York, 136pp.

Godshall, F.A., 1970, The analysis of cloud amount from satellite data. Trans. New York Acad. Sci., 436-453.

Hahn, C.J., S.G. Warren, J. London, R.H. Chervin and R. Jenne., 1984, Atlas of simultaneous occurrence of different cloud types over land, NCAR:TN-241-STR, NCAR Technical Note, National Center for Atmospheric Research, Boulder, Colorado, 21pp and 186 maps.

Hilsenrath, E., and B.M. Schlesinger, 1981, Total ozone seasonal and interannual variations derived from the 7 year Nimbus-4 BUV data set, J. Geophys.Res., 86, 12087-12096.

Liljas, E., 1984, Processed satellite imageries for operational forecasting, SMHI, Norrköping, Sweden, 43pp.

Malberg, H., 1973, Comparison of mean cloud cover obtained by satellite photographs and ground-based observations over Europe and the Atlantic, Mon. Weather Rev., 101, 893.

Merritt, E.S., 1966, On the reliability and representativeness of sky cover observation, J. Appl. Meteor., 5, 369.

Minnis, P., and E.F. Harrison, 1984a, Diurnal variability of regional cloud and clear sky radiative parameters derived from GOES data. Part I: Analysis method, J. Climate Appl. Meteor., 23, 993-1011.

Minnis, P., and E.F. Harrison, 1984b, Diurnal variability of regional cloud and clear sky radiative parameters derived from GOES data. Part II, November 1978 cloud distributions, J. Climate Appl. Meteor., 23, 1012-1031.

Minnis, P., and E.F. Harrison, 1984c, Diurnal variability of regional cloud and clear sky radiative parameters derived from GOES data. Part III, November 1978 radiative parameters, J. Climate Appl. Meteor., 23, 1032-1051.

Molnar, G., and J.A. Coakley, 1985, Retrieval of cloud cover from satellite imagery data: a statistical approach, J. Geophys. Res., 90, 12960-12970.

Phulpin, T., M. Derrien and A. Brard, 1983, A two-dimensional histogram procedure to analyse cloud cover from NOAA satellite high-resolution imagery. J. Climate Appl. Meteor., 22, 1332-1345.

Platt, C.M.R., 1983, On the bispectral method for cloud parameter determination from VISSR data: separating broken cloud and semi-transparent cloud, J. Climate Appl. Meteor., 22, 429-439.

Reynolds, D.W., and T.H. Vonder Haar, 1977, A bispectral method for cloud parameter determination, Mon. Weather Rev., 105, 446-457.

Rossow, W.B., F. Mosher, E. Kinsella, A. Arking, M. Desbois, E. Harrison, P. Minnis, E. Ruprecht, G. Seze, C. Simmer and E. Smith, 1985, ISCCP cloud algorithm intercomparison. J. Climate Appl. Meteor., 24, 877-903.

Saunders, R.W. and G.E. Hunt, 1980, METEOSAT observations of diurnal

variations of radiation budget parameters, Nature, 283, 645-647.

Saunders, R.W., 1986, An automated scheme for the removal of cloud contamination from AVHRR radiances over Western Europe, Int. J. Remote Sensing, 7, 867-886.

Schiffer, R.A. and Rossow, W.B., 1983, The International Satellite Cloud Climatology Project (ISCCP). The First Project of the World Climate Research Program, Bull. Amer. Meteor. Soc., 64, 779-784.

Schiffer, R.A. and Rossow, W.B., 1985, ISCCP global radiance data set: a new resource for climate research, Bull. Amer. Meteor. Soc., 66, 1498-1505.

Sèze, G., C. Belcour and M. Desbois, 1984, Cloud cover analysis using spectral and spatial characteristics of METEOSAT images, Prepr. from COSPAR, Toulouse, 1984.

Sèze, G., and M. Desbois, 1986, Cloud cover analysis on satellite images using spatial and temporal characteristics of the data, J. Climate Appl. Meteor., (in press).

Sèze, G., F. Drake, M. Desbois and A. Henderson-Sellers, 1986, Total and low cloud amounts over France and Southern Britain in the summer of 1983: comparison of surface-observed and satellite-retrieved values, Int. J. Remote Sensing, 7, 1031-1050.

Sèze, G., F. Drake, M. Desbois and A. Henderson-Sellers, 1987, Comparison of surface-observed and satellite-retrieved cloudiness over France and Southern Britain in the summer of 1983, J. Climate Appl. Meteor. (In press).

Shenk, W.E., and V.V. Salomonson, 1972, A simulation study exploring the effects of sensor spatial resolution on estimates of cloud cover from satellites, J. Appl. Meteor., 11, 214-220.

Simmer, C., E. Raschke and E. Ruprecht, 1982, A method for

determination of cloud properties from two-dimensional histograms, Ann.Meteor., 20, 57-69.

Smith, E.A., and T.H. Vonder Haar, 1983, A hybrid radiation balance/cluster analysis cloud retrieval technique. Presented at IAMAP Symposium on Interdependence of Clouds, Trace Substances, Radiation and Climate, IUGG 16th General Assembly, Hamburg, F.R. Germany, August 1983.

Wielicki, B.A., and R.M. Welch, 1986, Cumulus cloud properties derived using Landsat satellite data, J. Climate Appl. Meteor., 25, 261-276.

World Climate Programme, 1982, The International Satellite Cloud Climatology Project (ISCCP) preliminary implementation plan (Rev.1) WCP-35, World Meteorological Organisation, Geneva.

END

1-87

DTIC